inhibitor of ATF6, impaired cardiac function and increased the mortality rate at 14 days after MI. Furthermore, in transgenic mice, which expressed dominant negative mutant of ATF6, left ventricle was dilated and cardiac function was worse than wild-type littermates. In contrast, cardiac function after MI was better in transgenic mice, which expressed constitutively active form of ATF6, compared with wild-type littermates. These results suggest that ATF6 plays a crucial role in not only protecting cardiac remodeling under the pathological state but also maintaining cardiac function under the physiological state.

## 2. Materials and methods

### 2.1. Mice and surgical procedures

All experimental procedures were performed according to the guidelines established by Chiba University for experiments in animals and all protocols were approved by our institutional review board. We generated transgenic mice that expressed constitutively active mutant or dominant negative mutant of ATF6 in the heart [17]. A HA tag was inserted at the amino terminus just distal to the translational start site of the mutated ATF6 cDNA. The mutated cDNA was subcloned into murine α-myosin heavy chain (α-MHC) promoter-containing expression vector. The linearized DNA was injected into pronuclei of eggs from C57BL6 mice, and the eggs were transferred into the oviducts of pseudopregnant ICR mice. The transgene was identified by PCR with transgene-specific primers and by Southern blot analysis. Generation and genotyping of transgenic mice with cardiac-restricted overexpression of human Bcl-2 have been previously described [18]. The strain of Bcl-2 transgenic was mix-background between FVBN and C57BL/6. The wild-type littermates were served as controls for all studies. We anesthetized mice by intraperitoneally injecting 50 mg/kg pentobarbital sodium. Myocardial infarction (MI) was produced by ligation of the left anterior descending artery. To inhibit activation of ATF6, 4-(2-aminoethyl) benzenesulfonyl fluoride (AEBSF, 4.8 μg/g/day, Sigma, Saint Louis, MO) was continuously administered by osmotic minipump (DURECT, Cupertino, CA).

### 2.2. Echocardiography

Cardiac function was examined by echocardiogram (Vevo 660, VISUAL SONICS, Ontario, Canada) provided with a 25-MHz imaging transducer. All recordings were performed on conscious mice.

### 2.3. Histology

Hearts fixed in 10% formalin were embedded in paraffin, sectioned at 4 μm thickness, and stained with hematoxylin and eosin. For electron microscopic analysis, hearts were fixed in 4% paraformaldehyde containing 0.25% glutaraldehyde, postfixed in 1% osmium tetroxide, and embedded in Epon 812. Ultrathin sections were stained with uranyl acetate and lead citrate. For detection of apoptotic cells, TUNEL labeling was performed with an In Situ Apoptosis Detection kit (Takara, Shiga, Japan). We counted the numbers of TUNEL-positive cardiomyocytes and hematoxylin-stained nuclei in a whole section of each samples. To analyze the number of apoptotic cells in infarcted hearts, digital photographs were taken at magnification ×200, and 20 random high-power fields (HPF) from each heart samples were chosen and quantified in a blinded manner.

### 2.4. Western blot analysis

Whole cell lysates were resolved by SDS-polyacrylamide gel electrophoresis. Proteins were transferred onto a nitrocellulose transfer membrane (Whatman, Dassel, Germany). Western blot analysis was performed with antibodies against HA (Santa Cruz Biotechnology, Santa Cruz, CA), ATF6 (IMGENEX, San Diego, CA), BiP (Stressgen Bioreagents, Victoria, Canada), or actin (Sigma). Hybridizing bands were visualized using an ECL detection kit (GE Healthcare, Buckinghamshire, UK).

### 2.5. Cell culture

Cardiomyocytes were prepared from ventricles of 1-day-old Wistar rats and cultured in Dulbecco's modified Eagle's medium supplemented with 10% fetal bovine serum at 37 °C in a mixture of 95% air and 5% $CO_2$. Cardiomyocytes were exposed to $CoCl_2$ (100 μM, Sigma) with or without AEBSF (300 μM) for 24 h. HEK293 cells were transfected with an expression plasmid encoding mutant form of ATF6 using FuGENE6 (Roche, Indianapolis, IN). The HEK293 cells were exposed to tunicamycin (TM, 2 μg/mL, Sigma) for 6 h.

### 2.6. RNA extraction and quantitative RT-PCR analysis

Total RNA was isolated from the heart, neonatal cardiomyocytes or HEK293 cells with RNAZol-B (Molecular Research Center, Cincinnati, OH) according to the manufacturer's instructions. cDNA synthesis of 1 μg of RNA was carried out by using QuantiTect Reverse Transcription Kit (QIAGEN, Hilden, Germany). Quantitative real time (RT)-PCR was performed by using the LightCycler with Taqman Universal Probe Library and the Light Cycler Master (Roche).

### 2.7. Immunohistochemistry

Cardiomyocytes of neonatal rats cultured on glass cover slips were incubated with the antibody to α-actinin (Sigma), followed by incubation with Cy3-labeled secondary antibodies. Nuclei were counterstained with Hoechst 33258 dye. An antibody against HA was incubated with the paraffin sections of murine hearts, and immunoreactivity was evaluated using the avidin–biotin–peroxidase complex method (ScyTek Laboratories, Logan, UT). The reactions were optimized using diaminobenzidine chromogen (Vector Laboratories, Burlingame, CA) and were counterstained with hematoxylin.

### 2.8. Statistical analysis

Data are shown as mean ± s.e.m. Multiple group comparison was performed by one-way analysis of variance (ANOVA) followed by the Bonferroni procedure for comparison of means. Comparisons between two groups were analyzed by the two-tailed Student's *t*-test. Values of $P<0.05$ were considered statistically significant.

## 3. Results

### 3.1. ER stress response in the ischemic heart

To elucidate whether the ER stress is increased in the heart under stress conditions, we produced MI in wild-type mice. The mRNA and protein levels of BiP were increased from 1 to 4 days after MI, respectively (Fig. 1a and b). The protein levels of total (90 kDa, p90ATF6) and cleaved form (50 kDa, p50ATF6) of ATF6 and the mRNA levels of ATF6 were increased after MI (Fig. 1a and b). Furthermore, phosphorylation levels of PERK and its target protein eukaryotic initiation factor (eIF) 2α were increased at 1 and 4 days after MI, respectively (Supplemental Fig. 1a). Although phosphorylation levels of IRE1 were not significantly increased, levels of its activated form XBP1 were increased (Supplemental Fig. 1a and b). The mRNA levels of CHOP were also increased (Fig. 1b). CHOP is a transcription factor that regulates apoptosis-related factors under the ER stress condition. These results suggest that the ER stress response is induced in the heart after MI.

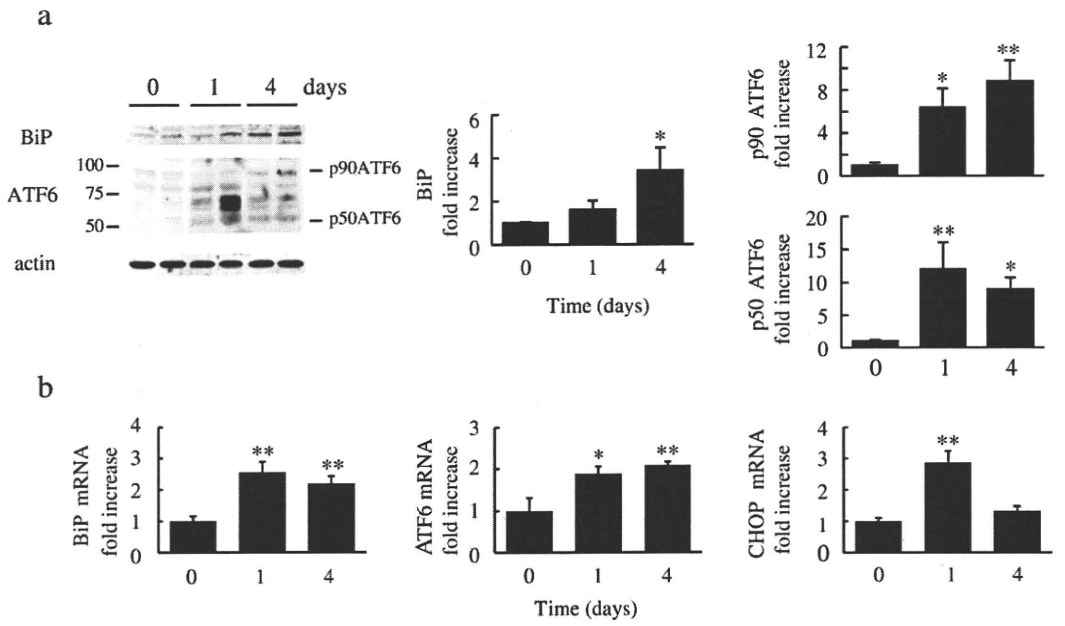


**Fig. 1.** ER stress response occurs in the ischemic heart. (a) Infarcted hearts during 4 days were analyzed for protein levels of BiP and total (p90ATF6) and cleaved form (p50ATF6) of ATF6 by Western blot analysis. Molecular mass makers (kDa) are indicated on the left. Quantification of BiP and ATF6 proteins as compared with sham (time = 0). $^{*}P<0.05$, $^{**}P<0.01$ versus day 0. $n=4$. (b) Expression levels of BiP, ATF6 and CHOP in hearts during 4 days of MI were quantified by RT-PCR analysis, normalized against GAPDH mRNA expression. $^{*}P<0.05$, $^{**}P<0.01$ versus day 0. $n=5$.

### 3.2. Inhibition of ATF6 in the ischemic heart

We examined the role of ATF6 in the ischemic heart using AEBSF, an ATF6 inhibitor [19]. We treated wild-type mice with AEBSF or vehicle and produced MI. The treatment with AEBSF was effective because it inhibited the cleavage of ATF6 (p50ATF6) in the ischemic heart (Fig. 2a). The survival rate after MI was much lower in mice treated with AEBSF than in mice treated with vehicle (Fig. 2b). In echocardiography, left ventricular posterior wall thickness was thinner, left ventricular dimension was larger and fractional shortening was smaller in mice treated with AEBSF than in mice treated with vehicle at 14 days after MI (Fig. 2c, Supplemental Table 1). These results suggest that ATF6 prevents cardiac remodeling after MI.

To clarify how AEBSF enhanced cardiac remodeling after MI, we examined expression levels of BiP, an ER chaperone which is induced by ATF6 and helps to refold unfolding proteins and ameliorates the ER stress [3,20]. mRNA levels of BiP were decreased in hearts by the treatment with AEBSF (Fig. 3a). Since it has been reported that overwhelming of the ER stress induces apoptosis, we examined apoptosis by TUNEL method. The number of TUNEL-positive cells was greater in AEBSF-treated group than in vehicle-treated group at 24 h after MI (Fig. 3b). Furthermore, expression level of CHOP was more strongly increased in AEBSF-treated group after MI (Fig. 3c). We exposed cultured cardiomyocytes to $CoCl_2$, a hypoxia mimetic, with or without AEBSF for 24 h. AEBSF augmented $CoCl_2$-induced cardiomyocyte apoptosis (Fig. 3d). To further clarify the role of ATF6 in cardiomyocytes under ischemic condition, we used a siRNA against rat ATF6. The siRNA decreased expression level of ATF6 in cardiomyocytes (Supplemental Fig. 2a), and augmented cardiomyocyte apoptosis (Supplemental Fig. 2b, lane 1 versus lane 3 and lane 5 versus lane 7). Next, we examined whether off target effects of AEBSF affect cardiomyocyte death. In the presence of the siRNA, AEBSF further increased the number of cardiomyocyte death (Supplemental Fig. 2b, lane 3 versus lane 4, lane 7 versus lane 8), suggesting that the effect of AEBSF on the heart is not only ATF6 inhibition but also some additional effects. These results suggest that inhibition of ATF6 increases ER stress-induced apoptotic death of cardiomyocytes in the ischemic heart, resulting in enhancement of cardiac remodeling after MI.

### 3.3. Role of dominant negative mutant of ATF6 in the heart

Pharmacological inhibition of ATF6 with AEBSF induced dilatation of left ventricle and depression of cardiac function even in sham-operated murine hearts (Fig. 2c), suggesting that ATF6 also plays a critical role in maintaining cardiac homeostasis under the physiological state. There are two forms of ATF6, ATF6α and ATF6β [21]. It has been reported that knockout mice of either ATF6α or ATF6β does not show significant phenotypes, while their double knockout mice are embryonic lethal [22,23]. Therefore, to define the role of ATF6 in the heart under the physiological state, we made transgenic mice (dnTg) that expressed a dominant negative mutant of ATF6 with HA tag under the control of α-MHC promoter (Fig. 4a) [17]. The dominant negative mutant of ATF6 has only a cytoplasmic domain of ATF6 and amino acids 315–317 of the cytoplasmic domain are changed from KNR to TAA. It has been reported that the mutant would be predicted to disrupt DNA-binding activity but dimerize with endogenous ATF6 and prevent its binding to ATF6 DNA-binding sites [17]. To confirm the effect of the mutant, we examined the expression levels of BiP in HEK293 cells transfected with the mutant. The mutant attenuated the increase of BiP expression levels by treatment of tunicamycin (TM), an ER stress inducer (Fig. 4b). Western blot analysis showed that HA was detected only in hearts of dnTg mice, and immunohistochemical analysis showed that the mutant was expressed at the nucleus of cardiomyocytes in dnTg mice (Fig. 4c). To examine whether the mutant acts as a dominant negative in vivo, we performed quantitative RT-PCR of ATF6-target genes such as BiP and ER degradation enhancing like protein 1 (EDEM1) [20,23]. The mRNA levels of BiP and EDEM1 were lower in hearts of dnTg mice compared with wild-type littermates (Fig. 4d). The survival rate was significantly lower in dnTg mice than wild-type littermates (Fig. 4e). The wall of left ventricle was thin and the cavity of hearts was dilated in dnTg mice (Fig. 4f). Echocardiographic analysis showed that left ventricular posterior wall thickness was thinner, left ventricular

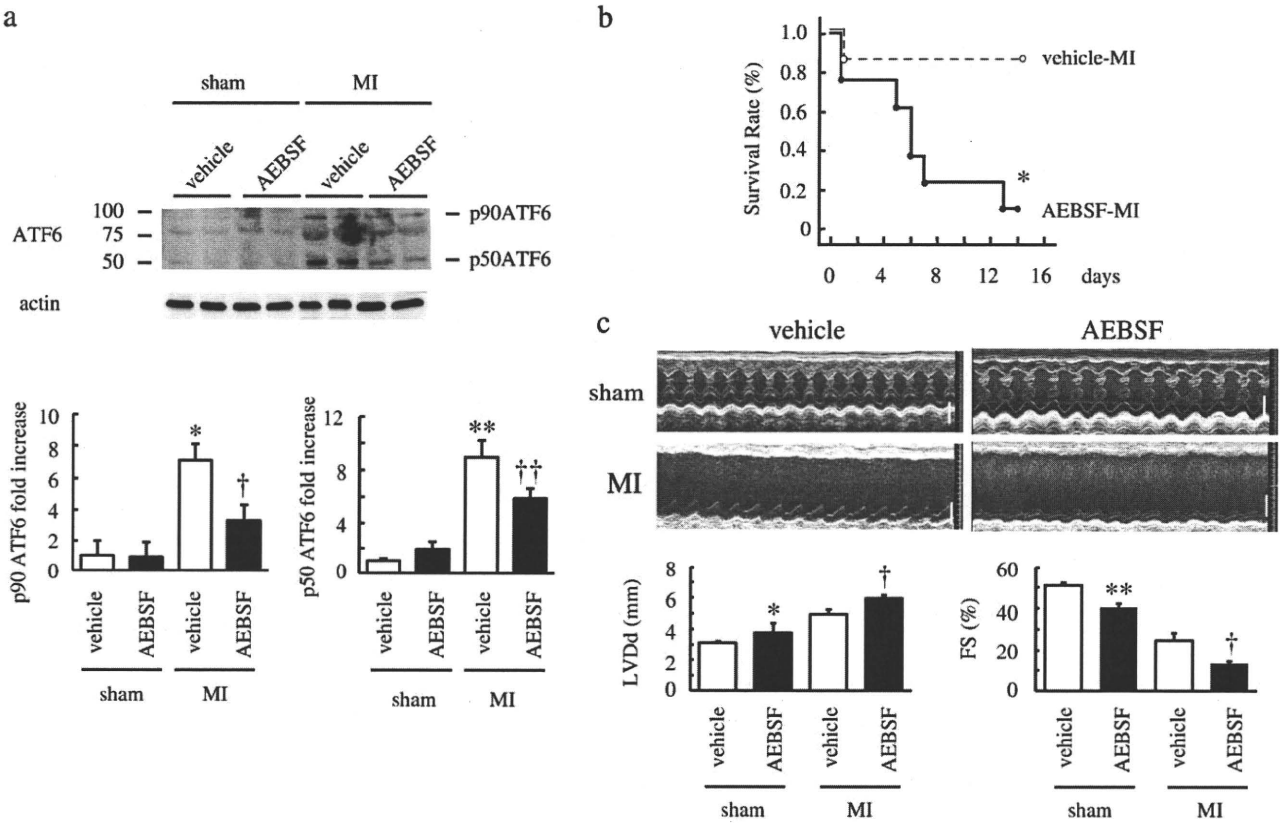


**Fig. 2.** AEBSF enhances cardiac remodeling after MI. (a) Sham-operated or infarcted hearts treated with vehicle or AEBSF were analyzed for protein levels of total (p90ATF6) and cleaved form (p50ATF6) of ATF6 by western blot analysis. Molecular mass makers (kDa) are indicated on the left. Quantification of ATF6 proteins as compared with sham-vehicle group. *$P<0.05$, **$P<0.01$ versus sham treated with vehicle. †$P<0.05$, ††$P<0.01$ versus MI treated with vehicle. $n=4$. (b) Kaplan–Meier survival curve after MI. *$P<0.05$ versus MI treated with vehicle. Vehicle, $n=10$; AEBSF, $n=23$. (c) Left ventricular end-diastolic dimension (LVDd) and fractional shortening (FS) were examined at 14 days after MI by echocardiogram. Scale bar, 2 mm. *$P<0.05$, **$P<0.01$ versus sham treated with vehicle. $P<0.01$ versus MI treated with vehicle.

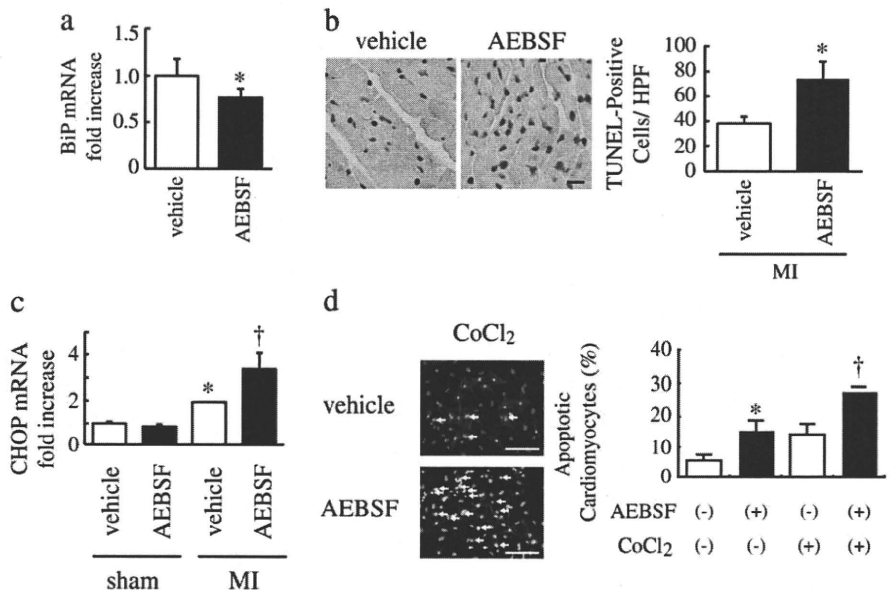


**Fig. 3.** AEBSF increases apoptotic cardiomyocytes. (a) Expression levels of BiP in sham-operated hearts were quantified by RT-PCR analysis, normalized against GAPDH mRNA expression. *$P<0.05$ versus vehicle. $n=5$. (b) TUNEL-positive cells (brown) in hearts at 24 h after MI. Scale bar, 10 μm. Quantitative analysis for TUNEL-positive cells at 24 h after MI. *$P<0.01$ versus vehicle. $n=4$. (c) Expression levels of CHOP in hearts of mice subjected with MI were quantified by RT-PCR analysis, normalized against GAPDH mRNA expression. *$P<0.05$ versus sham treated with vehicle. †$P<0.01$ versus MI treated with vehicle. $n=5$. (d) Cardiomyocytes were incubated with α-actinin (red), and nuclei were counterstained with Hoechst 33258 (blue). Arrows indicate condensed and Hoechst-stained nuclei indicative of apoptosis. The graph showed quantitative analysis for $CoCl_2$-induced apoptotic cardiomyocytes treated with vehicle or AEBSF. *$P<0.05$ versus non-treated cardiomyocytes. †$P<0.01$ versus $CoCl_2$-treated cardiomyocytes with vehicle. $n=5$. Scale bar, 100 μm.

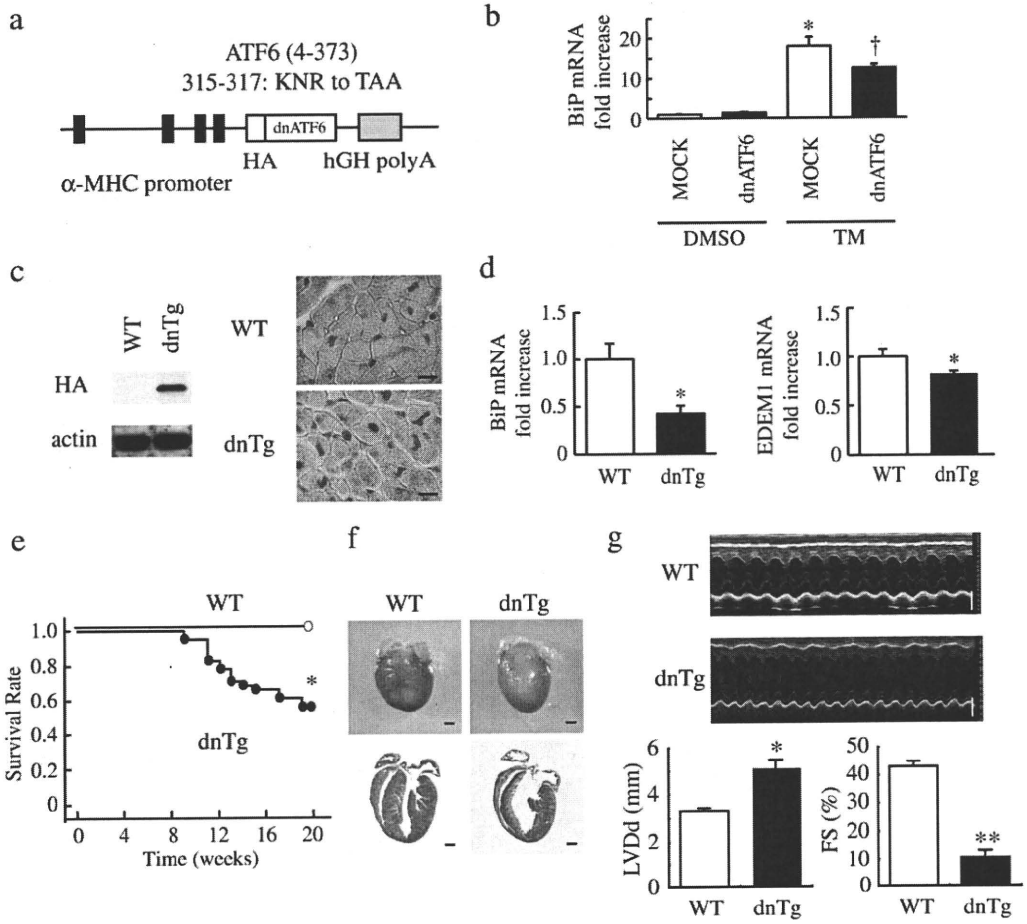


**Fig. 4.** The dominant negative mutant of ATF6 transgenic mice. (a) Schematic diagram represented the dominant negative mutant of ATF6 (dnATF6) transgene. HA-tagged dnATF6 was subcloned between the murine α-MHC promoter and human growth hormone (hGH) polyA. (b) Expression levels of BiP in HEK293 cells transfected with MOCK or an expression plasmid encoding the dominant negative mutant form of ATF6 were quantified by RT-PCR analysis, normalized against GAPDH mRNA expression. HEK293 cells were incubated with DMSO or TM for 6 h. *$P<0.01$ versus MOCK with DMSO, †$P<0.05$ versus MOCK with TM. $n=4$. (c) Western blot analysis and immunohistochemical staining (brown) for HA in hearts of wild-type littermates (WT) or dnTg mice at 8 weeks of age. Scale bar, 10 μm. (d) Expression levels of BiP and EDEM1 in hearts of WT or dnTg mice at 8 weeks of age were quantified by RT-PCR analysis, normalized against GAPDH mRNA expression. *$P<0.05$ versus WT. $n=4$. (e) Kaplan–Meier survival curve. *$P<0.05$ versus WT. WT, $n=19$; dnTg, $n=17$. (f) Gross morphology (upper images) and sections (lower images) of WT or dnTg murine hearts at 8 weeks of age. Scale bar, 1 mm. (g) Left ventricular end-diastolic dimension (LVDd) and fractional shortening (FS) were examined at 8 weeks of age by echocardiogram. Scale bar, 2 mm. *$P<0.05$, **$P<0.01$ versus WT.

dimension was larger and systolic function was impaired in dnTg mice compared with those in wild-type littermates (Fig. 4g, Supplemental Table 2). These results suggest that ATF6 is necessary to maintain cardiac function and structure under the physiological state.

Electron microscopic analysis showed that endoplasmic reticulums were expanded (Fig. 5a, 3 and I) and myofilaments were decreased (Fig. 5a, 4 and II) in cardiomyocytes of dnTg mice compared with wild-type littermates (Fig. 5a, 1 and 2). Expanded endoplasmic reticulums indicated that the ER stress was increased. Degenerated cardiomyocytes, suggesting apoptotic cardiomyocytes, were also observed in dnTg mice (Fig. 5a, 5 and III). Much more TUNEL-positive cardiomyocytes were observed in dnTg mice than in wild-type littermates (Fig. 5b). Furthermore, quantitative RT-PCR revealed that mRNA levels of ER stress-related apoptotic factors such as CHOP and p53 up-regulated modulator of apoptosis (PUMA) were upregulated in hearts of dnTg mice (Fig. 5c) [24,25]. To elucidate the role of cardiomyocyte apoptosis, we crossed dnTg mice and transgenic mice which overexpressed an anti-apoptotic protein Bcl-2 in cardiomyocytes [18]. Overexpression of Bcl-2 ameliorated dilatation of left ventricle and decrease of cardiac function (Fig. 5d, Supplemental Table 3), suggesting that ATF6 plays an important role in maintaining cardiac function and structure under the physiological state at least in part via inhibiting apoptosis of cardiomyocytes.

### 3.4. Role of constitutively active mutant of ATF6 in the heart

We next examined whether activation of ATF6 had protective effects on left ventricular remodeling after MI. Since only a cytoplasmic domain of ATF6 (aa1–373) activated expression of BiP gene (Fig. 6a) [16], we used this deletion mutant of ATF6 as a constitutively active form of ATF6. We generated transgenic mice (caTg) that expressed the cytoplasmic domain of ATF6 with HA tag under the control of α-MHC promoter (Fig. 6b) [17]. Western blot analysis showed that HA was detected only in hearts of caTg mice, and immunohistochemical analysis showed that the transgene was expressed at the nucleus of cardiomyocytes in caTg mice (Fig. 6c). There was no significant difference in heart size and cardiac function (Fig. 6d and e, Supplemental Table 4), suggesting that activation of ATF6 does not affect cardiac structure and function under the physiological state.

To examine whether activation of ATF6 had protective effects on the heart under the pathological state, we made MI in caTg mice. Echocardiographic study showed that left ventricular dimension was smaller and fractional shortening was better in caTg mice compared with in wild-type littermates at 14 days after MI (Fig. 6f). The number of TUNEL-positive cells was less in hearts of caTg mice than wild-type littermates at 24 h after MI (Fig. 6g). The survival rate was better in caTg

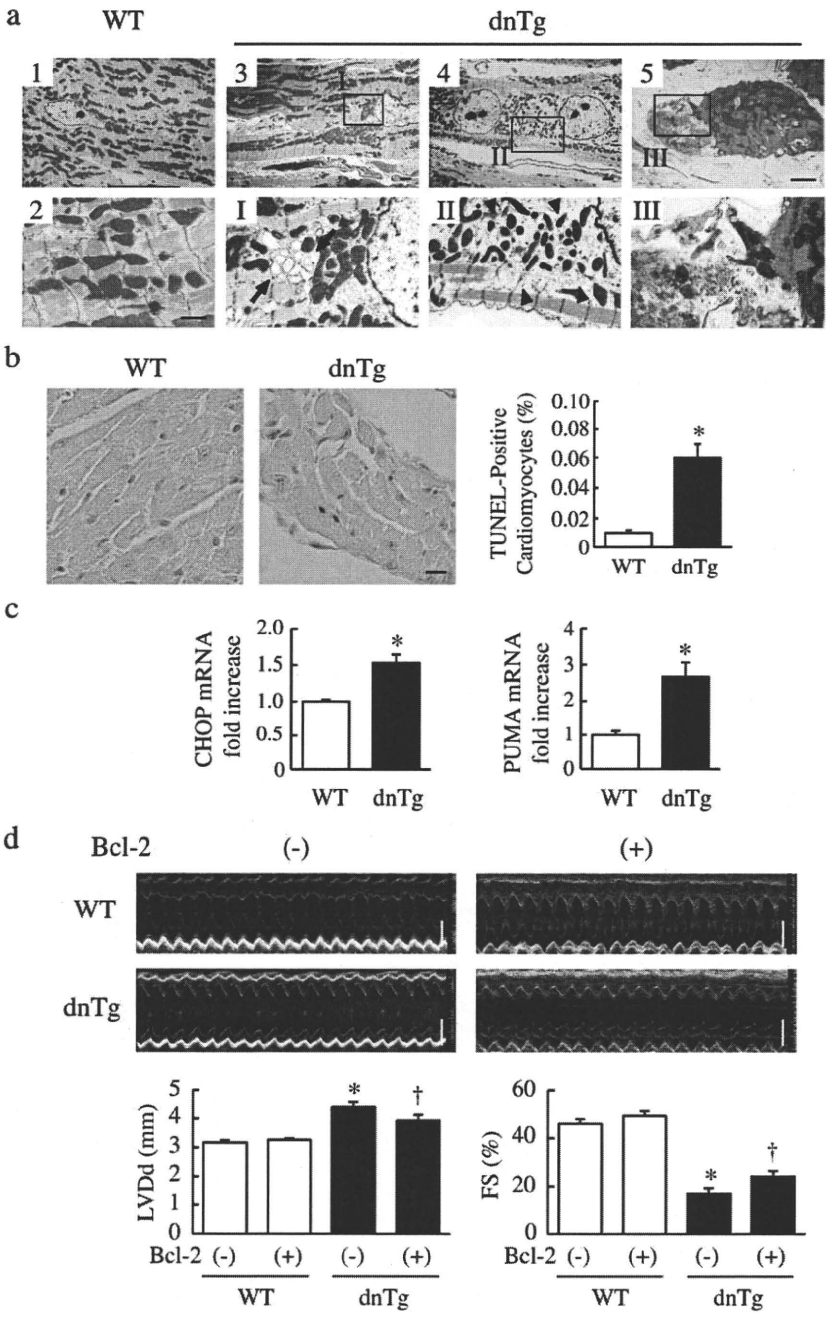


**Fig. 5.** Apoptotic cardiomyocytes are increased in dominant negative mutant of ATF6 transgenic mice. (a) Electron microscopic analysis. Endcoplasmic reticulums were expanded (arrow, 3 and I) and myofilaments were decreased (arrow head, 4 and II) in cardiomyocytes of dnTg mice. Degenerated cardiomyocytes were observed in dnTg mice (5 and III). Scale bar, 1 μm. WT, wild-type littermates. (b) TUNEL-positive cardiomyocytes (brown) in hearts of WT or dnTg mice. Scale bar, 10 μm. The graph showed quantitative analysis for TUNEL-positive cardiomyocytes at 8 weeks of age. *$P<0.05$ versus WT. $n=5$. Scale bar, 10 μm. (c) Expression levels of CHOP and PUMA in hearts of WT or dnTg mice were quantified by RT-PCR analysis, normalized against GAPDH mRNA expression. *$P<0.05$ versus WT. $n=4$. (d) Left ventricular end-diastolic dimension (LVDd) and fractional shortening (FS) were examined at 8 weeks of age by echocardiogram. Scale bar, 2 mm. *$P<0.01$ versus WT Bcl-2(−) mice, †$P<0.05$ versus dnTg Bcl-2(−) mice.

mice than in wild-type littermates even when they were treated with AEBSF (Supplemental Fig. 3a). On the other hand, the survival rate was lower in dnTg mice than in wild-type littermates (Supplemental Fig. 3b). These results suggest that activation of ATF6 has protective effects on cardiomyocytes and prevents cardiac remodeling after MI.

## 4. Discussion

Recent reports show that the ER stress response is activated in the heart exposed to prolonged stresses such as pressure overload [14] as well as acute stresses such as ischemia/reperfusion [26]. Although there is a report showing that BiP expression is detected in cardiomyocytes of border zone after MI [27], expressions of other ER stress-related factors are not known in hearts after MI. We revealed that all three branches of ER stress sensor, such as ATF6, PERK, and IRE1, were activated in the MI heart (Fig. 1, Supplemental Fig. 1). The mRNA and protein levels of an ER chaperone BiP, which is regulated by ATF6, were also increased (Fig. 1). Furthermore, the mRNA levels of CHOP were increased, which has been reported to induce apoptosis under excessive ER stress (Fig. 1b). These results suggest that the ER stress response is induced in the heart by MI and that excessive ER stress induces apoptosis of cardiomyocytes after MI.

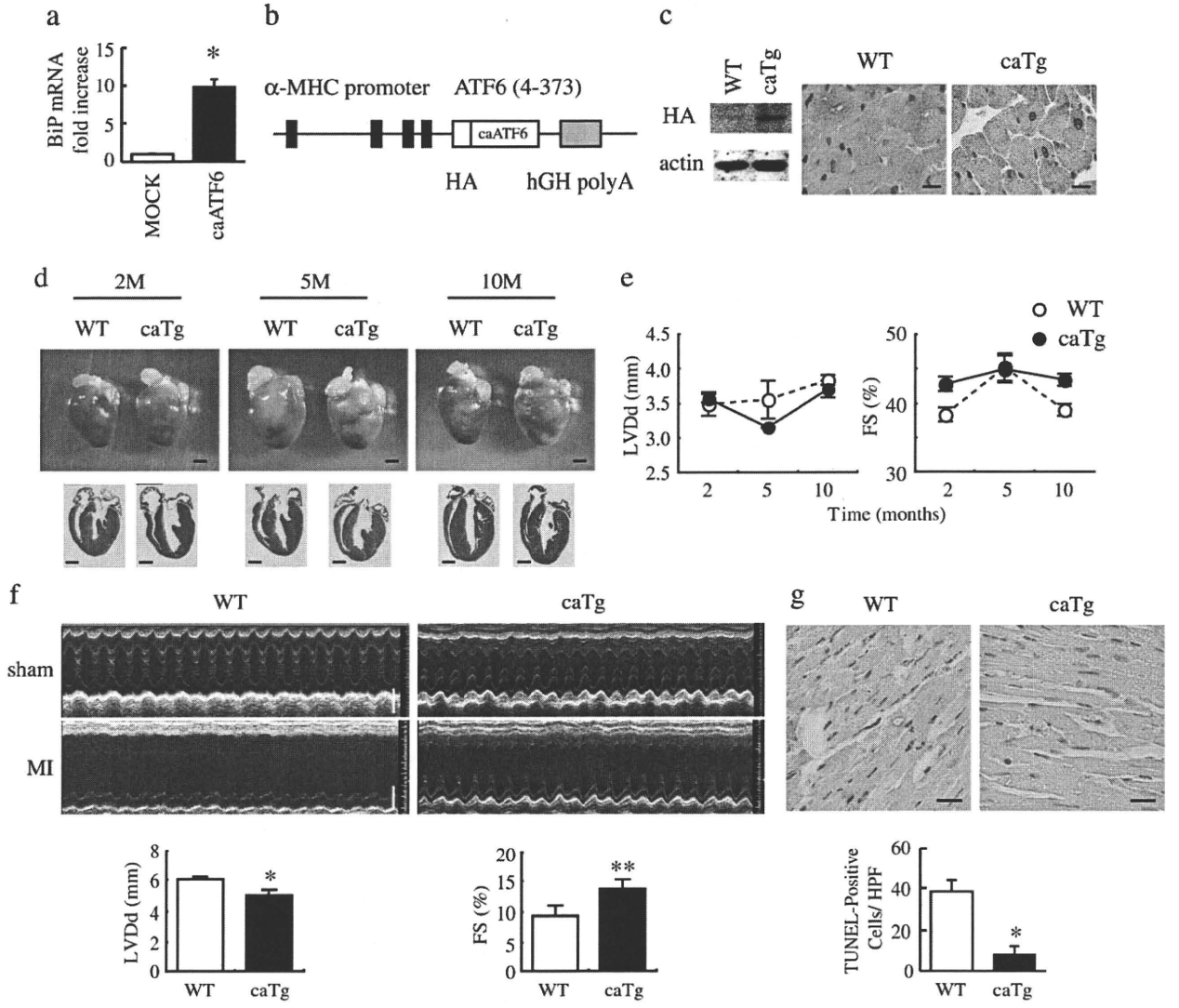


**Fig. 6.** The constitutively active mutant of ATF6 transgenic mice. (a) Expression levels of BiP in HEK293 cells transfected with MOCK or an expression plasmid encoding the constitutively active form of ATF6 were quantified by RT-PCR analysis, normalized against GAPDH mRNA expression. *$P<0.05$ versus MOCK. (b) Schematic diagram represented the constitutively active mutant of ATF6 (caATF6) transgene. HA-tagged caATF6 was subcloned between the murine α-MHC promoter and human growth hormone (hGH) polyA. (c) Western blot analysis and immunohistochemical staining (brown) for HA in hearts of wild-type littermates (WT) or caTg mice at 2 months of age. Scale bar, 10 μm. (d) Gross morphology (upper images) and sections (lower images) of WT or caTg murine hearts at 2, 5 and 10 months (M) of age. Scale bar, 1 mm. (e) Left ventricular end-diastolic dimension (LVDd) and fractional shortening (FS) were examined at 2, 5 and 10 months of age by echocardiogram. (f) Left ventricular end-diastolic dimension (LVDd) and fractional shortening (FS) were examined at 14 days after myocardial infarction by echocardiogram. Scale bar, 2 mm. *$P<0.05$, **$P<0.01$ versus WT. (g) TUNEL-positive cells (brown) in hearts at 24 h after MI. Scale bar, 10 μm. The graph showed quantitative analysis for TUNEL-positive cells at 24 h after MI. Scale bar, 100 μm. *$P<0.05$ versus vehicle. $n=3$.

ATF6 is a major transcription factor to induce gene expression of ER chaperones as well as ERAD components [22]. We firstly produced MI in wild-type mice in the presence of an ATF6 inhibitor, AEBSF. AEBSF has been reported to inhibit site-1 protease in vitro, which cleaves and activates ATF6 [19]. In this study, AEBSF inhibited an increase of activated forms of ATF6 (p50ATF6) after MI (Fig. 2a), suggesting that AEBSF indeed suppressed ATF6 function also in vivo. AEBSF reduced survival rate and worsened cardiac function after MI (Fig. 2b and c, Supplemental Table 1). Although it remains unclear how inhibition of ATF6 function deteriorated cardiac remodeling after MI, suppression of BiP might be one reason (Fig. 3a). BiP is a chaperone to reduce the ER stress, and a recent report shows that BiP has protective effects on cardiomyocytes against ischemic injury [28]. On the other hand, BiP null mice exhibit embryonic lethality because of an increase of apoptosis in the inner cell mass [29]. Suppression of BiP by AEBSF might increase apoptosis in the ischemic heart due to excessive ER stress, resulting in deterioration of cardiac remodeling. Indeed, the number of TUNEL-positive cells and expression level of CHOP were increased more in the MI heart by AEBSF treatment (Fig. 3b and c). The in vitro result that the number of CoCl2-induced apoptotic cardiomyocytes was increased more by AEBSF further supports this idea (Fig. 3day).

Targeted disruption of XBP1 gene is embryonic lethal in mice because of cardiac developmental defects [30]. Double knockout mice of ATF6α and ATF6β gene are also embryonic lethal [22]. On the other hand, PERK knockout mice exhibit death of pancreatic β cells and develop diabetes [12]. Although these studies suggest that the ER stress response is important for development and homeostasis of organs, the physiological role of the ER stress response in the heart has not been fully elucidated. To clarify the role of the ER stress response, especially ATF6 in the heart under physiological state, we established mice that expressed dominant negative mutant of ATF6 in the heart (Fig. 4a). Heart size was enlarged and cardiac function was impaired in dnTg mice even without pathological stresses (Fig. 4f and g, Supplemental Table 2), suggesting that ATF6 is necessary to maintain cardiac structure and function in adulthood.

Electron microscopic analysis showed that endoplasmic reticulum was expanded in cardiomyocytes of dnTg mice (Fig. 5a), suggesting that the ER stress is increased. The number of TUNEL-positive cardiomyocytes was increased (Fig. 5b) and mRNA levels of ER stress-induced apoptosis-related genes such as CHOP and PUMA were upregulated in the heart of dnTg mice (Fig. 5c). Impaired ER stress response by dominant negative mutant of ATF6 might increase apoptotic cardiomyocytes even under physiological state, resulting in cardiac dysfunction. This idea was supported by the result that overexpression of Bcl-2 significantly improved cardiac function in dnTg mice (Fig. 5d, Supplemental Table 3).

Cardiac remodeling after MI was prevented in caTg mice (Fig. 6f, Supplemental Table 5), and was deteriorated in dnTg mice (Supplementary Fig. 2b). Furthermore, the reduced survival rate with AEBSF was improved in caTg mice (Supplemental Fig. 2a). These results suggest that ATF6 activation after MI is protective in the heart, which is consistent with the recent result of ischemia/reperfusion injury in hearts [26]. Although the decrease of TUNEL-positive cells might be involved in the prevention of cardiac remodeling after MI (Fig. 6g), precise mechanisms of how overexpression of ATF6 ameliorates cardiac remodeling remain to be determined.

This study indicates that activation of the ER stress response factor ATF6 plays a critical role in protecting hearts under the pathological state and maintaining cardiac function under the physiological state.

## Acknowledgment

We thank R. Prywes (Columbia University, New York, NY) for a constitutively active and dominant negative mutants of ATF6 expression construct, M.D. Schneider (Imperial College, London, UK) for Bcl-2 transgenic mice and J. Robbins (Children's Hospital Research Foundation, Cincinnati, OH) for a fragment of α-MHC gene promoter. We thank E. Fujita, R. Kobayashi, Y. Ishiyama, I. Sakamoto, M. Ikeda, A. Furuyama and Y. Ohtsuki for technical support and M. Iiyama, K. Matsumoto, Y. Ishikawa and Y. Yasukawa for animal care.

Funding Sources: This work was supported by a Grant-in-Aid for Scientific Research on Priority Area and for Exploratory Research, Ministry of Education, Culture, Sports, Science and Technology (to I.K.).

## Appendix A. Supplementary data

Supplementary data associated with this article can be found, in the online version, at doi:10.1016/j.yjmcc.2010.03.020.

## References

[1] Frand AR, Cuozzo JW, Kaiser CA. Pathways for protein disulphide bond formation. Trends Cell Biol 2000;10:203–10.
[2] Gotoh T, Mori M. Nitric oxide and endoplasmic reticulum stress. Arterioscler Thromb Vasc Biol 2006;26:1439–46.
[3] Sitia R, Braakman I. Quality control in the endoplasmic reticulum protein factory. Nature 2003;426:891–4.
[4] Harding HP, Zhang Y, Ron D. Protein translation and folding are coupled by an endoplasmic-reticulum-resident kinase. Nature 1999;397:271–4.
[5] Brodsky JL, McCracken AA. ER protein quality control and proteasome-mediated protein degradation. Semin Cell Dev Biol 1999;10:507–13.
[6] Yoshida H. ER stress and diseases. FEBS J 2007;274:630–58.
[7] Kim R, Emi M, Tanabe K, Murakami S. Role of the unfolded protein response in cell death. Apoptosis 2006;11:5–13.
[8] Kaser A, Lee AH, Franke A, Glickman JN, Zeissig S, Tilg H, et al. XBP1 links ER stress to intestinal inflammation and confers genetic risk for human inflammatory bowel disease. Cell 2008;134:743–56.
[9] Duennwald ML, Lindquist S. Impaired ERAD and ER stress are early and specific events in polyglutamine toxicity. Genes Dev 2008;22:3308–19.
[10] Zhao L, Longo-Guess C, Harris BS, Lee JW, Ackerman SL. Protein accumulation and neurodegeneration in the woozy mutant mouse is caused by disruption of SIL1, a cochaperone of BiP. Nat Genet 2005;37:974–9.
[11] Oyadomari S, Koizumi A, Takeda K, Gotoh T, Akira S, Araki E, et al. Targeted disruption of the Chop gene delays endoplasmic reticulum stress-mediated diabetes. J Clin Invest 2002;109:525–32.
[12] Harding HP, Zeng H, Zhang Y, Jungries R, Chung P, Plesken H, et al. Diabetes mellitus and exocrine pancreatic dysfunction in perk-/- mice reveals a role for translational control in secretory cell survival. Mol Cell 2001;7:1153–63.
[13] Thameem F, Farook VS, Bogardus C, Prochazka M. Association of amino acid variants in the activating transcription factor 6 gene (ATF6) on 1q21-q23 with type 2 diabetes in Pima Indians. Diabetes 2006;55:839–42.
[14] Okada K, Minamino T, Tsukamoto Y, Liao Y, Tsukamoto O, Takashima S, et al. Prolonged endoplasmic reticulum stress in hypertrophic and failing heart after aortic constriction: possible contribution of endoplasmic reticulum stress to cardiac myocyte apoptosis. Circulation 2004;110:705–12.
[15] Shen J, Prywes R. ER stress signaling by regulated proteolysis of ATF6. Methods 2005;35:382–9.
[16] Haze K, Yoshida H, Yanagi H, Yura T, Mori K. Mammalian transcription factor ATF6 is synthesized as a transmembrane protein and activated by proteolysis in response to endoplasmic reticulum stress. Mol Biol Cell 1999;10:3787–99.
[17] Wang Y, Shen J, Arenzana N, Tirasophon W, Kaufman RJ, Prywes R. Activation of ATF6 and an ATF6 DNA binding site by the endoplasmic reticulum stress response. J Biol Chem 2000;275:27013–20.
[18] Tanaka M, Nakae S, Terry RD, Mokhtari GK, Gunawan F, Balsam LB, et al. Cardiomyocyte-specific Bcl-2 overexpression attenuates ischemia-reperfusion injury, immune response during acute rejection, and graft coronary artery disease. Blood 2004;104:3789–96.
[19] Okada T, Haze K, Nadanaka S, Yoshida H, Seidah NG, Hirano Y, et al. A serine protease inhibitor prevents endoplasmic reticulum stress-induced cleavage but not transport of the membrane-bound transcription factor ATF6. J Biol Chem 2003;278:31024–32.
[20] Adachi Y, Yamamoto K, Okada T, Yoshida H, Harada A, Mori K. ATF6 is a transcription factor specializing in the regulation of quality control proteins in the endoplasmic reticulum. Cell Struct Funct 2008;33:75–89.
[21] Haze K, Okada T, Yoshida H, Yanagi H, Yura T, Negishi M, et al. Identification of the G13 (cAMP-response-element-binding protein-related protein) gene product related to activating transcription factor 6 as a transcriptional activator of the mammalian unfolded protein response. Biochem J 2001;355:19–28.
[22] Yamamoto K, Sato T, Matsui T, Sato M, Okada T, Yoshida H, et al. Transcriptional induction of mammalian ER quality control proteins is mediated by single or combined action of ATF6alpha and XBP1. Dev Cell 2007;13:365–76.
[23] Wu J, Rutkowski DT, Dubois M, Swathirajan J, Saunders T, Wang J, et al. ATF6alpha optimizes long-term endoplasmic reticulum function to protect cells from chronic stress. Dev Cell 2007;13:351–64.
[24] Oyadomari S, Mori M. Roles of CHOP/GADD153 in endoplasmic reticulum stress. Cell Death Differ 2004;11:381–9.
[25] Nickson P, Toth A, Erhardt P. PUMA is critical for neonatal cardiomyocyte apoptosis induced by endoplasmic reticulum stress. Cardiovasc Res 2007;73:48–56.
[26] Martindale JJ, Fernandez R, Thuerauf D, Whittaker R, Gude N, Sussman MA, et al. Endoplasmic reticulum stress gene induction and protection from ischemia/reperfusion injury in the hearts of transgenic mice with a tamoxifen-regulated form of ATF6. Circ Res 2006;98:1186–93.
[27] Thuerauf DJ, Marcinko M, Gude N, Rubio M, Sussman MA, Glembotski CC. Activation of the unfolded protein response in infarcted mouse heart and hypoxic cultured cardiac myocytes. Circ Res 2006;99:275–82.
[28] Shintani-Ishida K, Nakajima M, Uemura K, Yoshida K. Ischemic preconditioning protects cardiomyocytes against ischemic injury by inducing GRP78. Biochem Biophys Res Commun 2006;345:1600–5.
[29] Luo S, Mao C, Lee B, Lee AS. GRP78/BiP is required for cell proliferation and protecting the inner cell mass from apoptosis during early mouse embryonic development. Mol Cell Biol 2006;26:5688–97.
[30] Reimold AM, Etkin A, Clauss I, Perkins A, Friend DS, Zhang J, et al. An essential role in liver development for transcription factor XBP-1. Genes Dev 2000;14:152–7.

Journal of Human Genetics (2011) 56, 47–51

www.nature.com/jhg

ORIGINAL ARTICLE

# SNPs on chromosome 5p15.3 associated with myocardial infarction in Japanese population

Asako Aoki[1,2], Kouichi Ozaki[1], Hiroshi Sato[3], Atsushi Takahashi[4], Michiaki Kubo[5], Yasuhiko Sakata[6], Yoshihiro Onouchi[1], Takahisa Kawaguchi[7], Tsung-Hsien Lin[8,9], Hitoshi Takano[2], Masahiro Yasutake[2], Po-Chao Hsu[8], Shiro Ikegawa[10], Naoyuki Kamatani[4], Tatsuhiko Tsunoda[7], Suh-Hang H Juo[11,12,13], Masatsugu Hori[6], Issei Komuro[6], Kyoichi Mizuno[2], Yusuke Nakamura[14] and Toshihiro Tanaka[1]

**Myocardial infarction (MI) occurs as the result of complex interactions of multiple genetic and environmental factors. By conducting a genome wide association study in a Japanese population using 210 785 single nucleotide polymorphism (SNP) markers, we identified a novel susceptible locus for MI on chromosome 5p15.3. An SNP (rs11748327) in this locus showed significant association in several independent cohorts (combined $P=5.3\times10^{-13}$, odds ratio=0.80, comparison of allele frequency). Association study using tag SNPs in the same linkage disequilibrium block revealed that two additional SNPs (rs490556 and rs521660) conferred risk of MI. These findings indicate that the SNPs on chromosome 5p15.3 are novel protective genetic factors against MI.**
*Journal of Human Genetics* (2011) **56,** 47–51; doi:10.1038/jhg.2010.141; published online 25 November 2010

**Keywords:** association; genome; myocardial infarction; SNP

## INTRODUCTION

Myocardial infarction (MI) leads to principal cause of death in developed countries. MI is characterized by the rapid development of coronary thrombosis following atherosclerotic plaque instability,[1] which leads to necrosis of myocardium and might result in sudden death. Despite the change in lifestyle and recent development of biomarkers, pharmacological intervention and percutaneous coronary intervention using drug eluting stents, the mortality is still high.

We started genome wide association studies (GWAS) of this disorder using nearly 90 000 gene-based single nucleotide polymorphisms (SNPs) (http://snp.ims.u-tokyo.ac.jp/)[2] by high-throughput multiplex-PCR invader assay system,[3] and identified several genes conferring risk of MI including *LTA*.[4–6] Although the roles of these susceptible genes in MI pathogenesis are under investigation, these findings showed the potent power of GWAS, which is hypothesis free, to identify unexpected anchors to further understand the disease. Through examining the LTA cascade by combination of biological and genetic analyses, we have identified additional MI susceptible genes.[7–9]

Genetic variants that confer susceptibility to MI have been indicated to be present on several chromosomal loci.[10–17] These studies, however, were conducted in individuals from European decent. Therefore, we carried out a systematic GWAS using 210 785 SNPs for MI in Japanese population. We report here identification of SNPs on chromosome 5p15.3 as a novel protective genetic factor against MI. We also examined Taiwanese population to see its universality in another population.

## MATERIALS AND METHODS

### DNA samples

For the genome wide association study and subsequent second-stage screening, MI case and control subjects (mixed cases with other diseases including asthma, breast cancer, lung cancer, hyperthyroidism, osteoporosis, chronic obstructive pulmonary disease, pollinosis and atopic dermatitis) were obtained from the BioBank Japan project (http://biobankjp.org/). The characteristics of the third, fourth cohorts and the diagnosis of define MI has been described previously.[8,9] For Taiwanese population, subjects were recruited from the Kaohsiung Medical University Hospital, Taiwan.[9] All Taiwanese subjects are of Chinese decent. All

[1]Laboratory for Cardiovascular Disease, Center for Genomic Medicine, RIKEN, Yokohama, Japan; [2]Division of Cardiology, Department of Medicine, Nippon Medical School, Tokyo, Japan; [3]School of Human Welfare Studies, Kwansei Gakuin University, Nishinomiya, Japan; [4]Laboratory for Statistical Analysis, Center for Genomic Medicine, RIKEN, Yokohama, Japan; [5]Laboratory for Genotyping Development, Center for Genomic Medicine, RIKEN, Yokohama, Japan; [6]Department of Cardiovascular Medicine, Osaka University Graduate School of Medicine, Suita, Japan; [7]Laboratory for Medical Informatics, Center for Genomic Medicine, RIKEN, Yokohama, Japan; [8]Division of Cardiology, Department of Internal Medicine, Kaohsiung Medical University Hospital, Kaohsiung, Taiwan; [9]Department of Internal Medicine, Kaohsiung Medical University, Kaohsiung, Taiwan; [10]Laboratory for Bone and Joint Disease, Center for Genomic Medicine, RIKEN, Tokyo, Japan; [11]Department of Medical Research, Kaohsiung Medical University Hospital, Kaohsiung, Taiwan; [12]Graduate Institute of Medical Genetics, Kaohsiung Medical University, Kaohsiung, Taiwan; [13]Center of Excellence for Environmental Medicine, Kaohsiung Medical University, Kaohsiung, Taiwan and [14]Center for Genomic Medicine, RIKEN, Yokohama, Japan
Correspondence: Dr T Tanaka, Laboratory for Cardiovascular Diseases, Center for Genomic Medicine, RIKEN, 1-7-22, Suehiro-cho, Tsurumi-ku, Yokohama, Kanagawa 230-0045, Japan.
E-mail: toshitan@src.riken.jp
Received 9 August 2010; revised 18 October 2010; accepted 20 October 2010; published online 25 November 2010

study subjects provided written informed consent to participation in this study, or if they were under 20 years old, their parents gave consent. Characteristics of the study subjects were summarized in Supplementary Table 1. The protocol was approved by the Ethical Committee at the Center for Genomic Medicine, The institute of physical and chemical research (RIKEN), Yokohama and of each participating institution and by the Internal Review Board of the Kaohsiung Medical University Hospital, Kaohsiung.

### SNP genotyping

The genotyping methods for GWAS and second-stage screening were described previously.[18] For third- and fourth-stage screening, we used multiplex-PCR invader assay described previously.[3] In the Taiwanese population, the SNPs were genotyped using the TaqMan SNP genotyping assay (Applied Biosystems, Foster City, CA, USA).

### Statistical analysis

Haplotype block and haplotype frequency were estimated using Haploview v4.0.[19] We used this software to select tag SNPs with a pairwise tagging mode and applied a permutation test for haplotype analysis. We also applied haplotype analysis using the program THESIAS[20] and conditional log-likelihood with Akaike information criterion (AIC): AIC=−2×(the maximized value of the conditional log-likelihood)+2×(the number of parameters). As the number of parameters, we used the number of alleles/haplotypes with frequencies >0.01 that were used for each model. In the logistic regression analysis of an SNP, we first applied a one degree of freedom (1 d.f.) likelihood ratio test to determine whether a 1-d.f. multiplicative allelic effects model of a 2-d.f. full genotype model was more appropriate.[20] As we found no significant difference from the full genotype model ($P>0.05$), we assumed a multiplicative allelic effects mode. Next, we performed a forward logistic regression analysis, where we started by assessing whether the most significant SNP was sufficient to model the association among the SNP set. For this, we used a 1-d.f. likelihood ratio test for adding each of the remaining SNPs to the model by assuming multiplicative allelic effects for the additional SNPs. Relationship between patients' clinical profile and genotype information were assessed by one-way analysis of variance and $\chi^2$-test.

### Northern blot analysis

Human multiple-tissue northern blots I, II (Clontech, Palo Alto, CA, USA) or First choice northern blot (Ambion, Austin, TX, USA) 1, 2 were pre-hybridized and hybridized with α-[$^{32}$P]-dCTP-labeled genomic fragments prepared by PCR using 106 primer pairs as probes (Primer pairs are listed in Supplementary Table 2). Washed membranes were exposed to bioimaging plate for 4–6 h. We detected signal with bioimaging analyzer (FLA7000, FUJIFILM, Tokyo, Japan) according to the manufacturer's instructions.

## RESULTS

### Genome wide association analysis

We performed staged GWAS that include three screening stages as shown in Figure 1. To avoid false-negative results, we set a very loose threshold in the first-stage screening. We first genotyped 268 068 SNPs with 194 MI cases and 1539 controls (first set of each MI and control) enrolled in BioBank Japan. We successfully obtained genotype information at 210 785 SNP loci. The genomic inflation factor (λ) was 1.03 on the basis of the *P*-values from the Cochran-Armitage trend test, indicating there is no population stratification. We then selected 8740 SNPs showing *P*-values <0.02 for the second-stage screening, and genotyped the second set of 1394 MI patients and 1425 control individuals (Supplementary Table 3). Distribution of *P*-values for these SNPs were summarized in Supplementary Table 4. We also assessed population stratification in second-stage samples by comparing with HapMap samples using principal component analyses,[21] and found that these samples did not show any sign of population stratification (Supplementary Figure 1). After the second-stage screening, we identified two SNPs showing statistical significance after

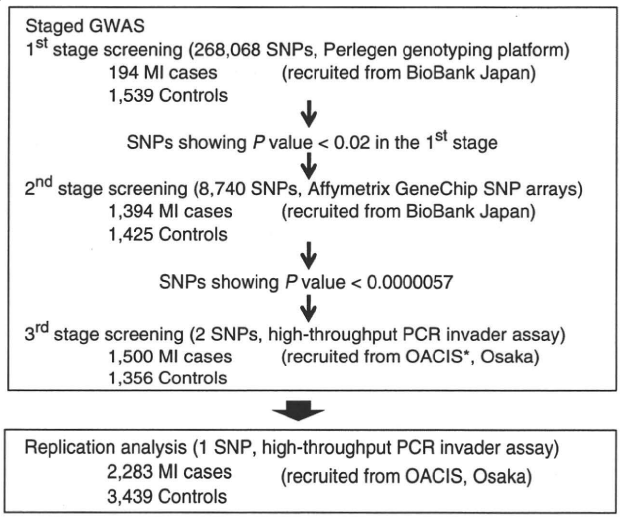


**Figure 1** Study design for the GWAS. *Osaka Acute Coronary Insufficiency Study group.

Bonferroni's correction (cutoff *P*-value<0.0000057). One SNP (rs3782886) was located within *BRAP* on chromosome 12q24 (Supplementary Table 3), previously reported to be associated with susceptibility to MI in two Asian populations.[9] The remaining SNP (rs11748327) on chromosome 5p15.3 showed *P*-value of $1.8\times10^{-6}$ in second-stage screening, and was verified by genotyping the third-stage samples (1500 cases and 1356 controls). Subsequent joint analyses for the associations of three panels showed the *P*-value with genome wide significance (combined $P=1.4\times10^{-9}$, odds ratio=0.77; Table 1). This association was further verified by replication panels with 2283 cases and 3439 controls (Table 1). Combined analysis of the four panels using Mantel–Haenszel test showed strong association of the SNP and MI, with a $\chi^2$ value of 56.0 ($P=5.3\times10^{-13}$; comparison of allele frequency) and odds ratio was 0.80 (95% confidence interval: 0.75–0.85; Table 1).

### Linkage disequilibrium and haplotype analysis

The marker SNP (rs11748327) was located within ~250 kb linkage disequilibrium (LD) block constructed on the basis of HapMap JPT data (http://www.hapmap.org)[22] using Haploview software[19] (Figure 2). To examine whether other genetic variation(s) in this block is associated with MI, we selected 15 tag SNPs in addition to rs11748327 from SNPs to have minor allele frequency >5% with pairwise tagging and $r^2$ threshold of 0.8. We compared allelic frequency of these SNPs in the third panel of each MI and control and found that two additional SNPs (rs490556 and rs521660) were significantly associated with MI after Bonfferoni's correction (Table 2).

The two SNPs, rs490556 and rs521660, were in LD to the marker SNP rs11748327 with $r^2$ of 0.59 and 0.79, respectively (Table 2). Then, we further genotyped the replication panel of 2283 cases and 3439 controls for the two SNPs and found again significant association between these SNPs and MI (Table 3). Two of the haplotypes based on these SNPs showed significant association with MI (Table 4). Therefore, we further examined the effect of these haplotypes by THESIAS[20] and observed a significant effect on disease susceptibility between the most and second-most frequent haplotypes that could be distinguished by rs490556. Considering the conditional log-likelihoods with AIC, indicating that rs490556 revealed smaller AIC value than the haplotype model, we assumed that rs490556 alone rather than the

**Table 1 Association of rs11748327 SNP with MI**

| | | *MI* | | | | | | | *Controls* | | | | | | | *Comparison of allele frequency* | | | |
|---|---|---|---|---|---|---|---|---|---|---|---|---|---|---|---|---|---|---|---|
| *Stage* | *Panel* | *11* | *%* | *12* | *%* | *22* | *%* | *SUM* | *11* | *%* | *12* | *%* | *22* | *%* | *SUM* | $\chi^2$ | *P-value* | *OR* | *95% CI* |
| Staged GWAS | 1st | 130 | 67.0 | 52 | 26.8 | 12 | 6.2 | 194 | 866 | 56.3 | 575 | 37.4 | 97 | 6.3 | 1538 | 5.5 | $1.9\times10^{-2}$ | 0.73 | 0.56–0.95 |
| | 2nd | 896 | 64.4 | 436 | 31.3 | 60 | 4.3 | 1392 | 758 | 55.3 | 531 | 38.7 | 82 | 6.0 | 1371 | 22.8 | $1.8\times10^{-6}$ | 0.74 | 0.83–0.65 |
| | 3rd | 938 | 62.8 | 480 | 32.1 | 76 | 5.1 | 1494 | 770 | 57.1 | 490 | 36.4 | 88 | 6.5 | 1348 | 10.2 | $1.4\times10^{-3}$ | 0.82 | 0.72–0.93 |
| | Combined | | | | | | | | | | | | | | | 40.7 | $1.4\times10^{-9}$* | 0.77 | 0.71–0.84 |
| Validation | Replication | 1437 | 62.9 | 740 | 32.4 | 106 | 4.6 | 2283 | 1964 | 57.5 | 1254 | 36.7 | 197 | 5.8 | 3415 | 16.7 | $4.4\times10^{-5}$ | 0.83 | 0.76–0.91 |
| | Combined | | | | | | | | | | | | | | | 56.0 | $5.3\times10^{-13}$* | 0.80 | 0.75–0.85 |

Abbreviations: CI, confidence interval; GWAS, genome wide association studies; MI, myocardial infarction; OR, odds ratio; SNP, single nucleotide polymorphism.
**P*-value was calculated by Mantel–Haenszel test.

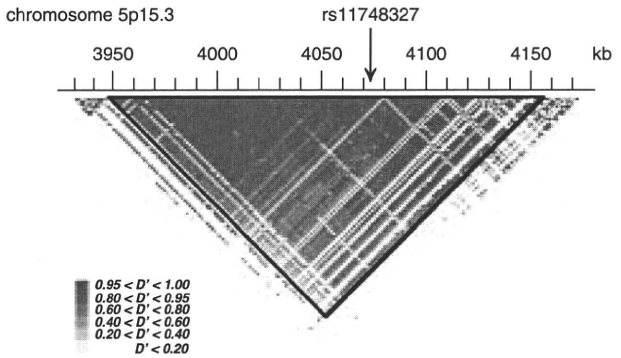


**Figure 2** LD (*D'*) block containing the marker SNP (rs11748327) on chromosome 5p15.3.

haplotypes well explained an association with MI. We also applied a logistic regression analysis to search for combinatorial effects of other SNPs to rs490556, but failed to find them. These results indicated that rs490556 itself or other SNPs with high LD to rs490556 are genetically associated with MI.

We also examined the possibility of confounding effect by age, sex and classical risk factors including diabetes, hypertension, smoking, hyperlipidemia within patients group using one-way analysis of variance and $\chi^2$ test, and found no relation between genotype and these factors (data not shown), indicating that the significant SNPs are an independent risk factor of MI.

We further conducted the association between the three tag SNPs and MI with ~550 cases and 800 controls from a Taiwanese population. However, the results were not consistent with the association for MI in Japanese population (Supplementary Table 5).

### Gene discovery at 5p15.3 locus

National Center for Biotechnology Information database (http://www.ncbi.nlm.nih.gov) contained only one expressed sequence tag, DA489076.1, in the genomic region within the LD block. Therefore, we examined expression of DA489076.1 in cDNA derived from 13 human tissues including heart, lung, liver, skeletal muscle, placenta, peripheral blood leukocyte, lymph node, adipose, aorta, brain, fetal brain, coronary artery smooth muscle and coronary artery endothelial cells. However, the expression was not detectable in all tissues examined (data not shown). To explore whether other unidentified transcripts are present in this genomic region, we examined mRNA expression in human adult tissues by northern blot analyses using 106 amplicons as probes (Primer pairs are listed in Supplementary Table 2) that cover the entire genomic region of the block except for repetitive sequences. We could not find obvious signal in all tissues examined (data not shown). Although we also examined micro-RNA (miRNA) and copy number variation databases (http://www.mirbase.org/search.shtml and https://gwas.lifesciencedb.jp/cgi-bin/cnvdb/cnv_top.cgi, respectively), we were not able to obtain any information for the genomic region.

## DISCUSSION

Through a GWAS in a Japanese population using 210 785 SNP markers, we identified SNPs on chromosome 5p15.3 as a novel protective genetic factor against MI. The association that we observed in the Japanese population could not be replicated in the Taiwanese population. This might be due to a lack of the power ($1-\beta$; 0.17 in comparison of allele frequencies for these SNPs) or genetic difference between the two populations. We also cannot exclude the possibility that other variants in this genomic region confer risk of MI in the Taiwanese population. The loci on chromosome 5p15.3 and *BRAP* were not detected in the previous GWAS from Europe and the United States; this failure may be due to the difference among ethnicity in allelic frequencies, which affects power of the study and also the effect size. Other reasons might include the ethnic difference in the precise LD pattern, possibility of unidentified hidden SNPs for Caucasian decent, various biases such as publication bias, leaving open the question of association in other populations for these loci.

We could not find replicated previous results for *LTA* and *PSMA6* in the first-stage screening. The estimated powers of the first-stage screening to replicate positive association for *LTA* and *PSMA6* were 0.28 and 0.24, respectively. The significant SNP in *LGALS2* was not on the SNP list of Perlegen genotyping system. Therefore, we think one of the reasons might be lack of the power of this study. Biases including publication bias, sampling bias, cannot be excluded. For chromosome 9p21 locus, the *P*-value in the first-stage screening was 0.0018 (rs1412834). At the second stage, it was 0.0098 and did not pass the threshold. As our aim did not include replication of the previous findings, threshold *P*-value at each screening stage was not appropriate for replication study.

In the genomic region of the LD block on chromosome 5p15.3, we were not able to detect any transcript by our analyses. It is possible we cannot detect unidentified some small non-coding RNAs <100 base pairs, particularly miRNAs. miRNA has important functions in gene regulation in animals and plants by binding to target sites in the 3′ untranslated regions on mRNAs of protein-coding genes to direct their posttranscriptional repression.[23] In fact, recent studies indicated that a single substitution in the mach of the miRNA seed to its target site can abolish gene repression.[24] SNPs in miRNA including pri-miRNAs, pre-miRNAs and mature miRNA could influence the processing and/or target selection of miRNAs and affect

**Table 2 Association analysis of the 15 tag SNPs with MI**

| | MI | | | | | | | Controls | | | | | | | | $r^2$ with |
|---|---|---|---|---|---|---|---|---|---|---|---|---|---|---|---|---|
| *dbSNP ID* | *11* | *%* | *12* | *%* | *22* | *%* | *SUM* | *11* | *%* | *12* | *%* | *22* | *%* | *SUM* | P-value[a] | *rs11748327* |
| rs511664 C>T | 1232 | 86.0 | 193 | 13.5 | 8 | 0.6 | 1433 | 1150 | 88.3 | 143 | 11.0 | 9 | 0.7 | 1302 | $1.6\times10^{-1}$ | 0.03 |
| rs505800 A>G | 763 | 51.4 | 599 | 40.3 | 123 | 8.3 | 1485 | 666 | 49.6 | 551 | 41.1 | 125 | 9.3 | 1342 | $4.0\times10^{-1}$ | 0.3 |
| rs2008927 C>T | 700 | 47.3 | 614 | 41.5 | 166 | 11.2 | 1480 | 650 | 49.2 | 524 | 39.6 | 148 | 11.2 | 1322 | $7.2\times10^{-1}$ | 0.18 |
| rs631942 G>A | 795 | 53.9 | 558 | 37.8 | 122 | 8.3 | 1475 | 660 | 48.9 | 569 | 42.1 | 121 | 9.0 | 1350 | $2.9\times10^{-1}$ | 0.4 |
| rs10060583 C>T | 566 | 38.1 | 686 | 46.2 | 233 | 15.7 | 1485 | 547 | 40.9 | 611 | 45.6 | 181 | 13.5 | 1339 | $9.1\times10^{-1}$ | 0.12 |
| rs490556 T>C | 863 | 58.1 | 521 | 35.1 | 102 | 6.9 | 1486 | 681 | 50.7 | 549 | 40.9 | 113 | 8.4 | 1343 | $2.4\times10^{-3}$ | 0.59 |
| rs521660 G>A | 762 | 55.3 | 515 | 37.3 | 102 | 7.4 | 1379 | 627 | 49.1 | 530 | 41.5 | 120 | 9.4 | 1277 | $1.5\times10^{-2}$ | 0.79 |
| rs1187466 T>A | 630 | 44.3 | 630 | 44.3 | 162 | 11.4 | 1422 | 579 | 46.9 | 540 | 43.8 | 115 | 9.3 | 1234 | $1.1\times10^{-1}$ | 0.11 |
| rs1187463 C>A | 743 | 50.4 | 600 | 40.7 | 130 | 8.8 | 1473 | 607 | 46.0 | 563 | 42.7 | 150 | 11.4 | 1320 | $7.5\times10^{-2}$ | 0.65 |
| rs903083 C>T | 1334 | 89.4 | 156 | 10.5 | 2 | 0.1 | 1492 | 1180 | 88.0 | 155 | 11.6 | 6 | 0.4 | 1341 | $2.6\times10^{-1}$ | 0.02 |
| rs10512709 G>A | 607 | 41.3 | 682 | 46.5 | 179 | 12.2 | 1468 | 559 | 42.3 | 611 | 46.3 | 151 | 11.4 | 1321 | $8.0\times10^{-1}$ | 0.17 |
| rs1187477 C>T | 1169 | 77.9 | 308 | 20.5 | 23 | 1.5 | 1500 | 1025 | 75.6 | 311 | 22.9 | 20 | 1.5 | 1356 | $3.0\times10^{-1}$ | 0.04 |
| rs1209069 C>T | 816 | 58.6 | 496 | 35.6 | 81 | 5.8 | 1393 | 779 | 61.2 | 435 | 34.2 | 58 | 4.6 | 1272 | $1.4\times10^{-1}$ | 0.04 |
| rs1493470 G>A | 827 | 55.9 | 566 | 38.3 | 86 | 5.8 | 1479 | 729 | 54.5 | 504 | 37.7 | 104 | 7.8 | 1337 | $2.4\times10^{-1}$ | 0.78 |
| rs1187483 T>C | 578 | 39.6 | 663 | 45.4 | 220 | 15.1 | 1461 | 478 | 36.0 | 635 | 47.8 | 215 | 16.2 | 1328 | $1.2\times10^{-1}$ | 0.41 |

Abbreviations: MI, myocardial infarction; SNP, single nucleotide polymorphism.
[a]Comparison of allelic frequency and adjusted for Bonferroni's correction.

**Table 3 Association of the rs490556 and rs521660 with MI**

| | | Cases | | | | | | | Controls | | | | | | | Comparison of allele frequency | | | |
|---|---|---|---|---|---|---|---|---|---|---|---|---|---|---|---|---|---|---|---|
| *dbSNP ID* | *Samples* | *11* | *%* | *12* | *%* | *22* | *%* | *Total* | *11* | *%* | *12* | *%* | *22* | *%* | *Total* | $\chi^2$ | P-value | *OR* | *95% CI* |
| rs490556 T>C | 3rd | 863 | 58.1 | 521 | 35.1 | 102 | 6.9 | 1486 | 681 | 50.7 | 549 | 40.879 | 113 | 8.4 | 1343 | 14.4 | $1.5\times10^{-4}$ | 0.79 | 0.70–0.89 |
| | Replication | 1324 | 58.4 | 802 | 35.4 | 141 | 6.2 | 2267 | 1786 | 51.9 | 1399 | 40.68 | 254 | 7.4 | 3439 | 20.6 | $5.7\times10^{-6}$ | 0.82 | 0.75–0.89 |
| | Combined | | | | | | | | | | | | | | | 33.8 | $4.0\times10^{-9*}$ | 0.81 | 0.76–0.87 |
| rs521660 G>A | 3rd | 762 | 55.3 | 515 | 37.3 | 102 | 7.4 | 1379 | 627 | 49.1 | 530 | 41.504 | 120 | 9.4 | 1277 | 10.9 | $9.4\times10^{-4}$ | 0.82 | 0.72–0.92 |
| | Replication | 1197 | 55.9 | 781 | 36.5 | 162 | 7.6 | 2140 | 1597 | 49.3 | 1342 | 41.445 | 299 | 9.2 | 3238 | 21.8 | $3.1\times10^{-6}$ | 0.81 | 0.75–0.89 |
| | Combined | | | | | | | | | | | | | | | 32.7 | $1.2\times10^{-8*}$ | 0.81 | 0.76–0.88 |

Abbreviations: CI, confidence interval; MI, myocardial infarction; OR, odds ratio; SNP, single nucleotide polymorphism.
*P-values were calculated by Mantel–Haenszel test.

**Table 4 Haplotype analysis**

| | SNP IDs<br>Risk allele | | | Haplotype frequency | | Comparison of haplotype frequency | |
|---|---|---|---|---|---|---|---|
| | *rs490556* | *rs11748327* | *rs521660* | *Case* | *Control* | $\chi^2$ | P-value |
| *Haplotype* | *T* | *C* | *G* | | | | |
| Haplotype 1 | T | C | G | 0.727 | 0.688 | 30.7 | $3.0\times10^{-8}$ |
| Haplotype 2 | C | T | A | 0.176 | 0.213 | 37.1 | $1.1\times10^{-9}$ |
| Haplotype 3 | C | C | A | 0.053 | 0.058 | 1.4 | $2.3\times10^{-1}$ |
| Haplotype 4 | T | T | A | 0.031 | 0.030 | 0.3 | $6.0\times10^{-1}$ |

Abbreviation: SNP, single nucleotide polymorphism.

miRNA-mediated translational suppression.[25] Therefore, the SNPs on chromosome 5p15.3 might be located within the region encoding unidentified miRNAs, affect their functions, and contribute to the development and/or progression of CAD. Although it is very difficult to reveal function of the SNP with the present knowledge, we think the increasing attention to function and/or higher-order structure of genome and subsequent progress will help to solve this problem.

We believe that knowledge of genetic factors contributing to its pathogenesis provides a useful clue for the development of diagnostic methods, treatments and preventive measures for this common but serious disorder.

## ACKNOWLEDGEMENTS

We thank Maki Takahashi, Mayumi Yoshii, Saori Kawakami, Rumiko Oishi, Makiko Matsuda, Taeko Nakajima and Michiko Nakamura for their assistance.

We also thank all the members of OACIS, the Rotary Club of Osaka-Midosuji District 2660 Rotary International and BioBank Japan for their contribution to the completion of our study. This work was conducted as a part of the BioBank Japan Project that was supported by the Ministry of Education, Culture, Sports, Sciences and Technology of the Japanese government. This work was also supported in part by grants from the Takeda science foundation, the Uehara science foundation, the Naito foundation, the Mitsubishi foundation, the Tokyo Biochemical Research foundation and NHRI-Ex96-9607PI (Taiwan).

1 Libby, P & Theroux, P Pathophysiology of coronary artery disease. *Circulation* **111,** 3481–3488 (2005).
2 Haga, H, Yamada, R, Ohnishi, Y, Nakamura, Y & Tanaka, T Gene-based SNP discovery as part of the Japanese Millennium Genome project; identification of 190 562 genetic variations in the human genome. *J. Hum. Genet.* **47,** 605–610 (2002).
3 Ohnishi, Y, Tanaka, T, Ozaki, K, Yamada, R, Suzuki, H & Nakamura, Y A high-throughput SNP typing system for genome-wide association studies. *J. Hum. Genet.* **46,** 471–477 (2001).
4 Ozaki, K, Ohnishi, Y, Iida, A, Sekine, A, Yamada, R, Tsunoda, T *et al.* Functional SNPs in the lymphotoxin-α gene that are associated with susceptibility to myocardial infarction. *Nat. Genet.* **32,** 650–654 (2002).
5 Ishii, N, Ozaki, K, Sato, H, Mizuno, H, Saito, S, Takahashi, A *et al.* Identification of a novel non-coding RNA, *MIAT*, that confers risk of myocardial infarction. *J. Hum. Genet.* **51,** 1087–1099 (2006).
6 Ebana, Y, Ozaki, K, Inoue, K, Sato, H, Iida, A, Lwin, H *et al.* A functional SNP in *ITIH3* is associated with susceptibility to myocardial infarction. *J. Hum. Genet.* **52,** 220–229 (2007).
7 Ozaki, K, Inoue, K, Sato, H, Iida, A, Ohnishi, Y, Sekine, A *et al.* Functional variation in *LGALS2* confers risk of myocardial infarction and regulates lymphotoxin-a secretion *in vitro*. *Nature* **429,** 72–75 (2004).
8 Ozaki, K, Sato, H, Iida, A, Mizuno, H, Nakamura, T, Miyamoto, Y *et al.* A functional SNP in *PSMA6* confers risk of myocardial infarction in the Japanese population. *Nat. Genet.* **38,** 921–925 (2006).
9 Ozaki, K, Sato, H, Inoue, K, Tsunoda, T, Sakata, Y, Mizuno, H *et al.* SNPs in *BRAP* associated with risk of myocardial infarction in Asian populations. *Nat. Genet.* **41,** 329–333 (2009).
10 Helgadottir, A, Thorleifsson, G, Manolescu, A, Gretarsdottir, S, Blondal, T, Jonasdottir, A *et al.* A common variant on chromosome 9p21 affects the risk of myocardial infarction. *Science* **316,** 1491–1493 (2007).
11 McPherson, R, Pertsemlidis, A, Kavaslar, N, Stewart, A, Roberts, R, Cox, D R *et al.* A common allele on chromosome 9 associated with coronary heart disease. *Science* **316,** 1488–1491 (2007).
12 Samani, N J, Erdmann, J, Hall, A S, Hengstenberg, C, Mangino, M, Mayer, B, *et al.* WTCCC and the Cardiogenics Consortium Genome-wide association analysis of coronary artery disease. *N. Engl. J. Med.* **357,** 443–453 (2007).
13 Wellcome Trust Case Control Consortium. Genome-wide association study of 14 000 cases of seven common diseases and 3000 shared controls. *Nature* **447,** 661–678 (2007).
14 Erdmann, J, Großhennig, A, Braund, P S, König, I R, Hengstenberg, C, Hall, A S, *et al.* Italian Atherosclerosis, Thrombosis, and Vascular Biology Working Group; Myocardial Infarction Genetics Consortium; Wellcome Trust Case Control Consortium; Cardiogenics Consortium New susceptibility locus for coronary artery disease on chromosome 3q22.3. *Nat. Genet.* **41,** 280–282 (2009).
15 Gudbjartsson, D F, Bjornsdottir, U S, Halapi, E, Helgadottir, A, Sulem, P, Jonsdottir, G M *et al.* Sequence variants affecting eosinophil numbers associate with asthma and myocardial infarction. *Nat. Genet.* **41,** 342–347 (2009).
16 Myocardial Infarction Genetics Consortium. Genome-wide association of early-onset myocardial infarction with single nucleotide polymorphisms and copy number variants. *Nat. Genet.* **41,** 334–341 (2009).
17 Trégouët, D A, König, I R, Erdmann, J, Munteanu, A, Braund, P S, Hall, A S, *et al.* Wellcome Trust Case Control Consortium; Cardiogenics Consortium Genome-wide haplotype association study identifies the *SLC22A3-LPAL2-LPA* gene cluster as a risk locus for coronary artery disease. *Nat. Genet.* **41,** 283–285 (2009).
18 Unoki, H, Takahashi, A, Kawaguchi, T, Hara, K, Horikoshi, M, Andersen, G *et al.* SNPs in *KCNQ1* are associated with susceptibility to type 2 diabetes in East Asian and European populations. *Nat. Genet.* **40,** 1098–1102 (2008).
19 Barrett, J C, Fry, B, Maller, J & Daly, M J Haploview: analysis and visualization of LD and haplotype maps. *Bioinformatics* **21,** 263–265 (2005).
20 Tregouet, D A & Garelle, V A new JAVA interface implementation of THESIAS: testing haplotype effects in association studies. *Bioinformatics* **23,** 1038–1039 (2007).
21 Price, A L, Patterson, N J, Plenge, R M, Weinblatt, M E, Shadick, N A & Reich, D Principal components analysis corrects for stratification in genome-wide association studies. *Nat. Genet.* **38,** 904–909 (2006).
22 The International HapMap Consortium. A haplotype map of the human genome. *Nature* **437,** 1299–1320 (2005).
23 Rinn, J L, Kertesz, M, Wang, J K, Squazzo, S L, Xu, X, Brugmann, S A *et al.* Functional demarcation of active and silent chromatin domains in human HOX loci by noncoding RNAs. *Cell* **129,** 1311–1323 (2007).
24 Brennecke, J, Stark, A, Russell, R B & Cohen, S M Principles of microRNA-target recognition. *PloS Biol.* **3,** e85 (2005).
25 Duan, R, Pak, C & Jin, P Single nucleotide polymorphism associated with mature miR-125a alters the processing of pri-miRNA. *Hum. Mol. Genet.* **16,** 1124 (2007).

Supplementary Information accompanies the paper on Journal of Human Genetics website (http://www.nature.com/jhg)

# Docking Protein Gab1 Is an Essential Component of Postnatal Angiogenesis After Ischemia via HGF/c-Met Signaling

Wataru Shioyama, Yoshikazu Nakaoka, Kaori Higuchi, Takashi Minami, Yoshiaki Taniyama, Keigo Nishida, Hiroyasu Kidoya, Takashi Sonobe, Hisamichi Naito, Yoh Arita, Takahiro Hashimoto, Tadashi Kuroda, Yasushi Fujio, Mikiyasu Shirai, Nobuyuki Takakura, Ryuichi Morishita, Keiko Yamauchi-Takihara, Tatsuhiko Kodama, Toshio Hirano, Naoki Mochizuki, Issei Komuro

***Rationale:*** **Grb2-associated binder (Gab) docking proteins, consisting of Gab1, Gab2, and Gab3, have crucial roles in growth factor–dependent signaling. Various proangiogenic growth factors regulate angiogenesis and endothelial function. However, the roles of Gab proteins in angiogenesis remain elusive.**

***Objective:*** **To elucidate the role of Gab proteins in postnatal angiogenesis.**

***Methods and Results:*** **Endothelium-specific Gab1 knockout (Gab1ECKO) mice were viable and showed no obvious defects in vascular development. Therefore, we analyzed a hindlimb ischemia (HLI) model of control, Gab1ECKO, or conventional Gab2 knockout (Gab2KO) mice. Intriguingly, impaired blood flow recovery and necrosis in the operated limb was observed in all of Gab1ECKO, but not in control or Gab2KO mice. Among several proangiogenic growth factors, hepatocyte growth factor (HGF) induced the most prominent tyrosine phosphorylation of Gab1 and subsequent complex formation of Gab1 with SHP2 (Src homology-2–containing protein tyrosine phosphatase 2) and phosphatidylinositol 3-kinase subunit p85 in human endothelial cells (ECs). Gab1-SHP2 complex was required for HGF-induced migration and proliferation of ECs via extracellular signal-regulated kinase (ERK)1/2 pathway and for HGF-induced stabilization of ECs via ERK5. In contrast, Gab1-p85 complex regulated activation of AKT and contributed partially to migration of ECs after HGF stimulation. Microarray analysis demonstrated that HGF upregulated angiogenesis-related genes such as *KLF2* (Krüppel-like factor 2) and *Egr1* (early growth response 1) via Gab1-SHP2 complex in human ECs. In Gab1ECKO mice, gene transfer of vascular endothelial growth factor, but not HGF, improved blood flow recovery and ameliorated limb necrosis after HLI.**

***Conclusion:*** **Gab1 is essential for postnatal angiogenesis after ischemia via HGF/c-Met signaling. (*Circ Res*. 2011; 108:664-675.)**

**Key Words:** angiogenesis ■ Gab1 ■ growth factors ■ endothelial cells ■ signal transduction

The Grb2-associated binder (Gab) family docking proteins, consisting of Gab1, Gab2, and Gab3, are involved in amplification and integration of signal transduction evoked by growth factors, cytokines, antigens, and numerous other molecules.[1,2] Gab proteins lack enzymatic activity but become phosphorylated on tyrosine residues, providing binding sites for multiple Src homology-2 (SH2) domain-containing proteins such as SH2 containing protein tyrosine phosphatase 2 (SHP2), phosphatidylinositol 3-kinase regulatory subunit p85, phospholipase Cγ, Crk, and GC-GAP. Docking of Gab proteins to SHP2 and p85 is considered to be essential for activation of mitogen activated protein kinase (MAPK), such as extracellular signal-regulated kinase (ERK)1/2 and AKT, respectively.[1,2] Conventional Gab1 knockout (Gab1KO) mice

Original received September 8, 2010; revision received January 20, 2011; accepted January 24, 2011. In December 2010, the average time from submission to first decision for all original research papers submitted to *Circulation Research* was 14.5 days.

From the Departments of Cardiovascular Medicine (W.S., Y.N., K.H., Y.A., T. Hashimoto, T. Kuroda, K.Y.-T., I.K.), Clinical Gene Therapy (Y.T., R.M.), and Advanced Cardiovascular Therapeutics (T. Kuroda), Osaka University Graduate School of Medicine, Suita; Research Center for Advanced Science and Technology (T.M., T. Kodama), University of Tokyo, Laboratory for System Biology and Medicine; Laboratory for Cytokine Signaling (K.N., T. Hirano), RIKEN Research Center for Allergy and Immunology, Yokohama; Department of Signal Transduction (H.K., H.N., N.T.), Research Institute for Microbial Diseases, Osaka University, Suita; Departments of Cardiac Physiology (T.S., M.S.) and Cell Biology (N.M.), National Cerebral and Cardiovascular Center Research Institute, Suita; Department of Clinical Pharmacology and Pharmacogenomics (Y.F.), Osaka University Graduate School of Pharmaceutical Sciences, Suita; and Laboratory of Developmental Immunology (T. Hirano), JST-CREST, Graduate School of Frontier Biosciences and Graduate School of Medicine, and WPI Immunology Frontier Research Center, Osaka University, Suita, Japan.

This manuscript was sent to Kathy Griendling, Consulting Editor, for review by expert referees, editorial decision, and final disposition.

Correspondence to Issei Komuro, MD, PhD, or Yoshikazu Nakaoka, MD, PhD, Department of Cardiovascular Medicine, Osaka University Graduate School of Medicine, 2-2, Yamadaoka, Suita, Osaka, 565-0871, Japan. E-mail komuro-tky@umin.ac.jp or ynakaoka@imed3.med.osaka-u.ac.jp



*Circulation Research* **is available at http://circres.ahajournals.org** **DOI: 10.1161/CIRCRESAHA.110.232223**

display embryonic lethality with impaired development of heart, placenta, skin, and skeletal muscle.[3,4] Conventional Gab2 knockout (Gab2KO) mice do not show any obvious developmental defects, but display impaired allergic responses, osteoclast defects, and abnormal hematopoiesis in adulthood.[5–7] Gab3 knockout mice exhibit no obvious phenotype.[8] Because Gab1KO mice are embryonic lethal, we and others created conditional knockout mice of Gab1 using the *Cre-loxP* system.[9–12] We created cardiomyocyte-specific Gab1/Gab2 double knockout mice and reported that Gab1 and Gab2 have the redundant roles for maintenance of cardiac function via neuregulin-1/ErbB signaling.[11]

Angiogenesis, the process of new blood vessel formation, is involved in many physiological and pathological settings such as ischemia, atherosclerosis, diabetes, and cancer.[13] During angiogenic growth, some endothelial cells (ECs) within capillary vessel wall are selected for "sprouting" and acquire invasive and motile behaviors. The tip cells, which lead the growing sprout, are guided by vascular endothelial growth factor (VEGF) gradients. The migration and proliferation of ECs behind the tip promote sprout extension. Fusion processes at the EC-EC interfaces establish a continuous lumen and blood flow promote maturation processes such as the "stabilization" of cell junctions and tight pericyte recruitment.[14,15] The angiogenic growth consists of these multistep processes from "endothelial sprouting" to "endothelial stabilization." ERK5 has been reported to have a central role for flow-mediated stabilization via upregulation of endothelial stabilization factor Krüppel-like factor (KLF)2.[16,17] However, the molecular mechanism how ERK5-KLF2 pathway is activated in in vivo angiogenesis remains unclear to date.

We reported an important role of Gab1 for ERK5 activation in gp130-dependent cardiomyocyte hypertrophy.[18,19] On the other hand, it has been reported that Gab1 has a role for VEGF-dependent signaling in the in vitro experiments using ECs.[20–22] However, the in vivo role of Gab proteins in angiogenesis has not been addressed to date. Here, we demonstrate that Gab1 in the vascular endothelium is essential for postnatal angiogenesis after ischemia. Endothelium-specific deletion of Gab1 results in enhanced propensity to limb necrosis after hindlimb ischemia (HLI) caused by impaired angiogenesis via hepatocyte growth factor (HGF)/c-Met signaling. On the contrary, global deletion of Gab2, another Gab protein expressed in the vascular endothelium, does not lead to limb necrosis and impairment of blood flow recovery after HLI compared with control mice. Consistently, Gab1, but not Gab2, is required for activation of ERK1/2, ERK5, and AKT after stimulation with HGF in ECs. Gab1 associates with SHP2 and p85 after stimulation with HGF in ECs. Gab1-SHP2 complex positively regulates migration and proliferation of ECs via ERK1/2 and contributes to stabilization of ECs via ERK5 presumably in association with upregulation of KLF2.

## Methods

An expanded Methods section is available in the Online Data Supplement at http://circres.ahajournals.org.

**Non-standard Abbreviations and Acronyms**

| | |
|---|---|
| **β-gal** | β-galactosidase |
| **CA** | constitutively active |
| **DN** | dominant-negative |
| **EC** | endothelial cell |
| **Egr** | early growth response |
| **ERK** | extracellular signal-regulated kinase |
| **FGF** | fibroblast growth factor |
| **Gab** | Grb2-associated binder |
| **Gab1ECKO** | endothelium-specific Gab1 knockout |
| **Gab1KO** | conventional Gab1 knockout |
| **Gab2KO** | conventional Gab2 knockout |
| **GST** | glutathione *S*-transferase |
| **HGF** | hepatocyte growth factor |
| **HLI** | hindlimb ischemia |
| **HUVEC** | human umbilical vein endothelial cell |
| **KLF** | Krüppel-like factor |
| **LDBF** | laser Doppler blood flow |
| **MACS** | Magnetic Cell Sorting |
| **MAPK** | mitogen activated protein kinase |
| **MEF2C** | myocyte enhancer factor 2 |
| **MEK** | mitogen activated protein kinase/extracellular signal-regulated kinase |
| **SHP2** | Src homology-2–containing protein tyrosine phosphatase 2 |
| **siRNA** | small interfering RNA |
| **TM** | thrombomodulin |
| **VEGF** | vascular endothelial growth factor |

### Animals

*Gab1*$^{flox}$ mice were generated in 129/Sv-C57BL/6J mixed background as described previously.[11] *Tie2-Cre* transgenic mice in CD-1 background were provided from Dr Thomas N. Sato.[23] Endothelium-specific Gab 1 knockout (Gab1ECKO) mice were generated by crossing *Gab1*$^{flox/flox}$ mice with *Tie2-Cre* transgenic mice. The creation of Gab2KO (*Gab1*$^{flox/flox}$ Gab2$^{-/-}$) mice were also described previously.[11] All the animals used for the experiments were 7- to 8-week-old male mice maintained on a 129/Sv-C57BL/6J-CD-1 mixed background. We housed all animals in a virus-free facility on a 12-hour light/12-hour dark cycle and fed them a standard mouse food. All experiments were carried out under the guidelines of Osaka University Committee for animal and rDNA experiments and were approved by the Osaka University Institutional Review Board.

## Results

### Generation of Endothelium-Specific Gab1 Knockout Mice

To elucidate the functional role of Gab1 in the endothelium, we first generated Gab1ECKO mice using the *Cre-loxP* system. We created a *Gab1*$^{flox}$ allele by introducing 2 *loxP* sites into introns flanking exon 2 which encodes part of the pleckstrin homology domain as described previously.[11] To cause recombination of the floxed allele exclusively in EC lineage, mice homozygous for the *Gab1-loxP*-targeted allele (*Gab1*$^{flox/flox}$) were crossed with transgenic mice expressing *Tie2* promoter-driven *Cre* recombinase (*Tie2-Cre* mice).[23] We created Gab1ECKO (*Gab1*$^{flox/flox}$ Tie2-Cre(+)) mice by crossing

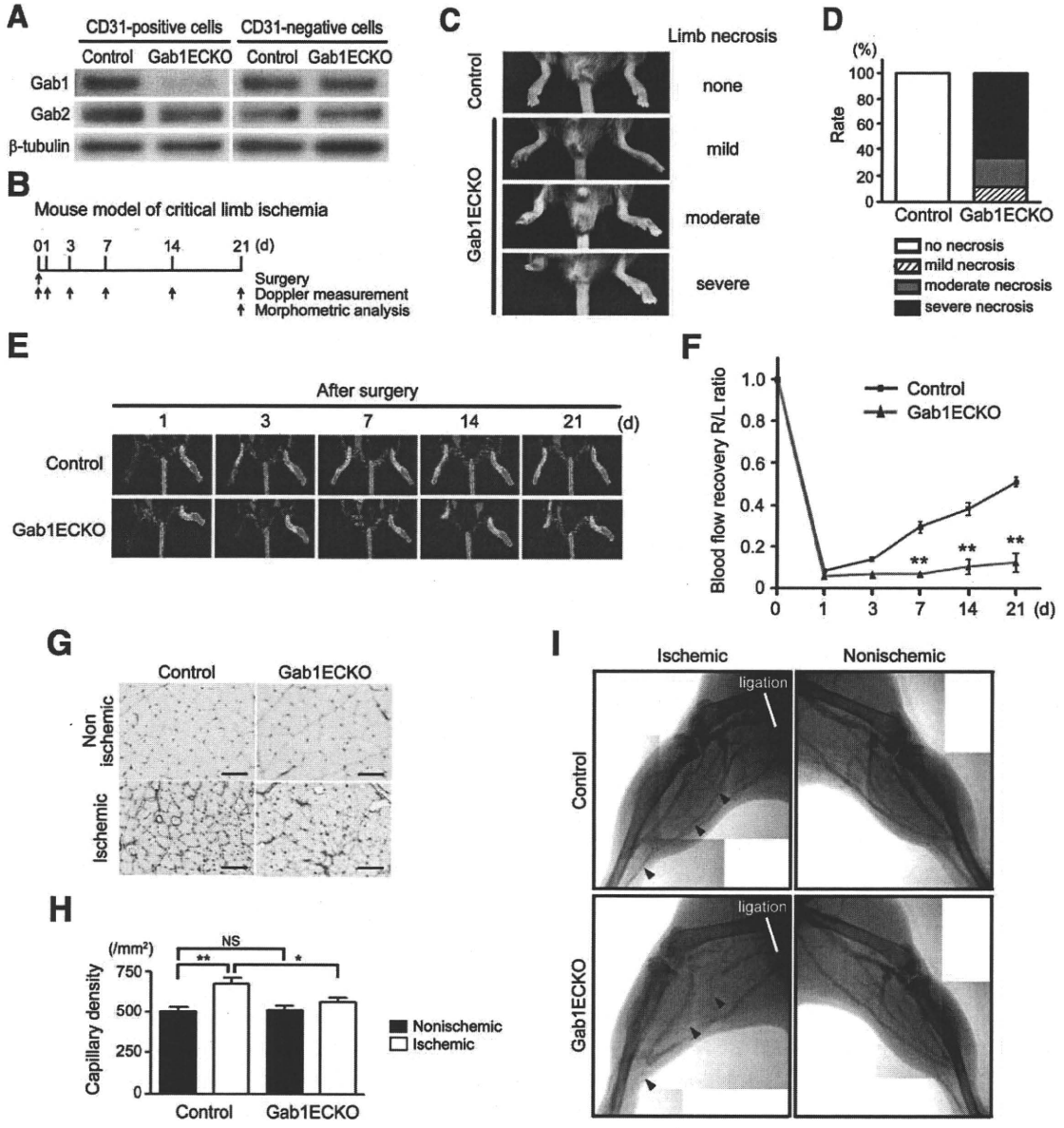


**Figure 1. Impaired blood flow recovery and angiogenesis in Gab1ECKO mice. A,** Gab1 was successfully ablated in the ECs in Gab1ECKO mice. The CD31-positive ECs were purified from the limb muscles using the MACS system. Whereas the expression of both Gab1 and Gab2 in the CD31-negative cells was almost comparable between the 2 groups, the expression of Gab1 was exclusively depleted in the CD31-positive cells in Gab1ECKO, but not in control mice. The expression levels of both Gab2 and β-tubulin were comparable between 2 groups. **B,** HLI was induced and blood flow of ischemic **(right)** and nonischemic **(left)** limb were measured on gastrocnemius muscle before and on the indicated days after surgery using LDBF analyzer. Tissues were harvested on day 21. **C,** All of Gab1ECKO mice showed limb necrosis after HLI, whereas control mice displayed no necrosis. **D,** Gross morphology of the ischemic limb was assessed on day 21 after surgery. **E,** Representative LBDF images of a mouse HLI on day1, 3, 7, 14, and 21 after surgery. **Red** represents greater flow; **blue,** less flow. **F,** Quantitative analysis of blood flow recovery after HLI expressed as ischemic **(right)** to nonischemic **(left)** LDBF ratio in control (n=9) and Gab1ECKO mice (n=9). Values are shown as means±SEM. $^{**}P<0.01$ vs control. **G,** Representative CD31 staining of capillaries from sections of nonischemic and ischemic adductor muscles. **Scale bar,** 100 μm. **H,** Quantitative analysis of capillary density in control and Gab1ECKO mice (number per high-power field; ×400 magnification). Values are shown as means±SEM. $^{*}P<0.05$, $^{**}P<0.01$ for the indicated groups. **I,** Arteriogenesis was determined by barium sulfate casting followed by x-ray microangiography. Three weeks after femoral artery ligation, mice were anesthetized and subjected to barium sulfate perfusion. Collateral artery growth is significantly attenuated in Gab1ECKO mice compared with control mice as indicated by arrowheads.

*Gab1*$^{+/flox}$ Tie2-Cre(+) mice with *Gab1*$^{flox/flox}$ mice. The offspring of these crossings were obtained at expected Mendelian ratios as follows: *Gab1*$^{flox/flox}$ Tie2-Cre(+) (n=23; 24.5%); *Gab1*$^{flox/flox}$ (n=27; 28.7%); *Gab*$^{+/flox}$ Tie2-Cre(+) (n=24; 25.5%); *Gab1*$^{flox/flox}$ (n=20; 21.3%).

To confirm the knockout of Gab1 protein in the vascular endothelium, the CD31-positive ECs were purified from the limb muscles of control (*Gab1*$^{flox/flox}$) and Gab1ECKO mice using the Magnetic Cell Sorting (MACS) system (Miltenyi Biotec Inc). The lysates of either purified CD31-positive ECs or CD31-negative cells were subjected to immunoblotting analyses. We confirmed successful depletion of Gab1 protein in CD31-positive ECs derived from Gab1ECKO mice, but not from control mice (Figure 1A). We also confirmed that

Gab1 expression in CD31-negative cells was almost comparable between control and Gab1ECKO mice (Figure 1A). There was no significant difference in Gab2 expression between control and Gab1ECKO mice both in CD31-positive ECs and CD31-negative cells (Figure 1A).

Next, we examined whether Gab1ECKO mice show vascular developmental abnormalities by whole-mount immunohistochemical staining with anti-CD31 antibody. Gab1ECKO mice did not show any obvious developmental vascular defects both during embryogenesis and at 8 weeks of age compared with control mice (Online Figure I, A through H). In addition, we crossed control ($Gab1^{flox/flox}$) mice with $Gab2^{-/-}$ mice to create $Gab1^{flox/flox}$ $Gab2^{-/-}$ mice, designated as Gab2KO mice. Gab2KO mice did not show any obvious vascular developmental defects at birth almost similarly as Gab1ECKO mice (data not shown).

## Gab1 in the Vascular Endothelium Is Essential for Postnatal Angiogenesis and Arteriogenesis After Ischemia

To determine the role of Gab1 and Gab2 in postnatal angiogenesis, control, Gab1ECKO, and Gab2KO male mice were subjected to HLI that was created by unilateral femoral artery ligation and analysis at different time points as diagrammed in Figure 1B. From day 7 to 21 after surgery, all of Gab1ECKO mice showed various grades of limb necrosis, whereas no necrotic phenotypes were observed in control and Gab2KO mice (Figure 1C and 1D; Online Figure II, A and B). To precisely determine functional defects in Gab1ECKO mice, blood flow of ischemic and nonischemic limb perfusion were measured before and on 1, 3, 7, 14, and 21 days after surgery using laser Doppler blood flow (LDBF) analyzer. Blood flows on the basal condition and on day 1 after surgery were comparable among mice from each group. Compared with the nonischemic limb, blood flow recovery of the ischemic limb was also comparable between control and Gab2KO mice (Online Figure II, C and D). These findings indicate that Gab2 is not critically engaged in blood flow recovery after HLI. In clear contrast, blood flow recovery in Gab1ECKO mice was substantially impaired on 7, 14, and 21 days (Figure 1E and 1F). These results indicate that endothelial Gab1 has a crucial role for blood flow recovery in response to HLI.

The improvement in blood flow recovery mainly corresponds to increased tissue capillary densities on day 21 after HLI (Figure 1G and 1H). The capillary densities in the nonischemic adductor muscles were comparable between control and Gab1ECKO mice (Figure 1G and 1H). On the other hand, control mice showed increased capillary densities in the ischemic adductor muscles, whereas Gab1ECKO mice exhibited no significant increase in capillary densities (Figure 1G and 1H). These findings indicate that Gab1, but not Gab2, has an essential role for blood flow recovery via the angiogenic response to HLI.

We also examined ischemia-initiated arteriogenesis in control and Gab1ECKO mice by barium sulfate casting followed by x-ray angiographic analysis. Interestingly, Gab1ECKO mice showed a significantly attenuated collateral formation compared with control mice (Figure 1I). These data suggest that Gab1 might have a critical role not only in angiogenesis but also in arteriogenesis after HLI.

## HGF Induces the Strongest Tyrosine Phosphorylation of Gab1 and Gab2 in the ECs

Several proangiogenic factors have been reported to regulate angiogenesis after ischemia. To elucidate how Gab1 is involved in the angiogenic response in the vascular endothelium, we performed in vitro experiments using human umbilical vein ECs (HUVECs). We first examined the expression of Gab family transcripts by RT-PCR and detected the mRNA of Gab1 and Gab2, but not that of Gab3 in HUVECs and human aortic ECs (Figure 2A). To examine which ligand induces tyrosine phosphorylation of Gab1 in HUVECs, cells were stimulated with proangiogenic factors such as HGF, VEGF, and fibroblast growth factor (FGF)2. Among these, HGF induced the strongest tyrosine phosphorylation of Gab1 and the subsequent complex formation of Gab1 with SHP2 and p85 in HUVECs (Figure 2B). We confirmed this result using 2 antibodies recognizing Gab1 only if phosphorylated on Tyr-627 or Tyr-307. Figure 2D and 2E show that both residues are strongly phosphorylated in response to HGF stimulation of HUVECs. We also examined the tyrosine phosphorylation of Gab2, another Gab family protein expressed in HUVECs, after stimulation with HGF, VEGF, or FGF2. HGF induced strong tyrosine phosphorylation of Gab2 and the subsequent complex formation of Gab2 with SHP2 and p85 in HUVECs, almost similarly as that of Gab1 (Figure 2C). Thus, Gab1 and Gab2 undergo strong tyrosine phosphorylation on HGF stimulation, suggesting that Gab1 and Gab2 might have a role for HGF-dependent signaling in HUVECs.

We also examined activation of downstream signaling pathways of Gab proteins after stimulation with HGF, VEGF, or FGF2. Among these, HGF induced the strongest and the most sustained activation of ERK1/2 and AKT in HUVECs (Figure 2D, 2F, and 2G). We previously reported that Gab1 is critically involved in activation of ERK5 after stimulation with leukemia inhibitory factor in cardiomyocytes.[18,19] Therefore, we performed ERK5 in vitro kinase assay using glutathione *S*-transferase (GST) fusion protein containing transactivating domain of myocyte enhancer factor 2 (MEF2C) (GST-MEF2C) as a substrate. HGF induced the strongest activation of ERK5 in HUVECs among these agonists (Figure 2H and 2I). Collectively, HGF induces the strongest activation of ERK1/2, AKT, and ERK5 in HUVECs, indicating that Gab family proteins might have an important role for full activation of these downstream pathways in HUVECs.

## Gab1, But Not Gab2, Is Required for Activation of ERK1/2, AKT, and ERK5 After Stimulation With HGF in HUVECs

To examine the role of Gab1 and Gab2 in HGF-dependent signaling pathway, we performed small interfering (si)RNA-mediated knockdown of Gab1 and Gab2 in HUVECs. We observed successful depletion of Gab1 or Gab2 protein in HUVECs 48 hours after transfection with the Gab1- or Gab2-specific siRNA, respectively (Figure 3A). The speci-

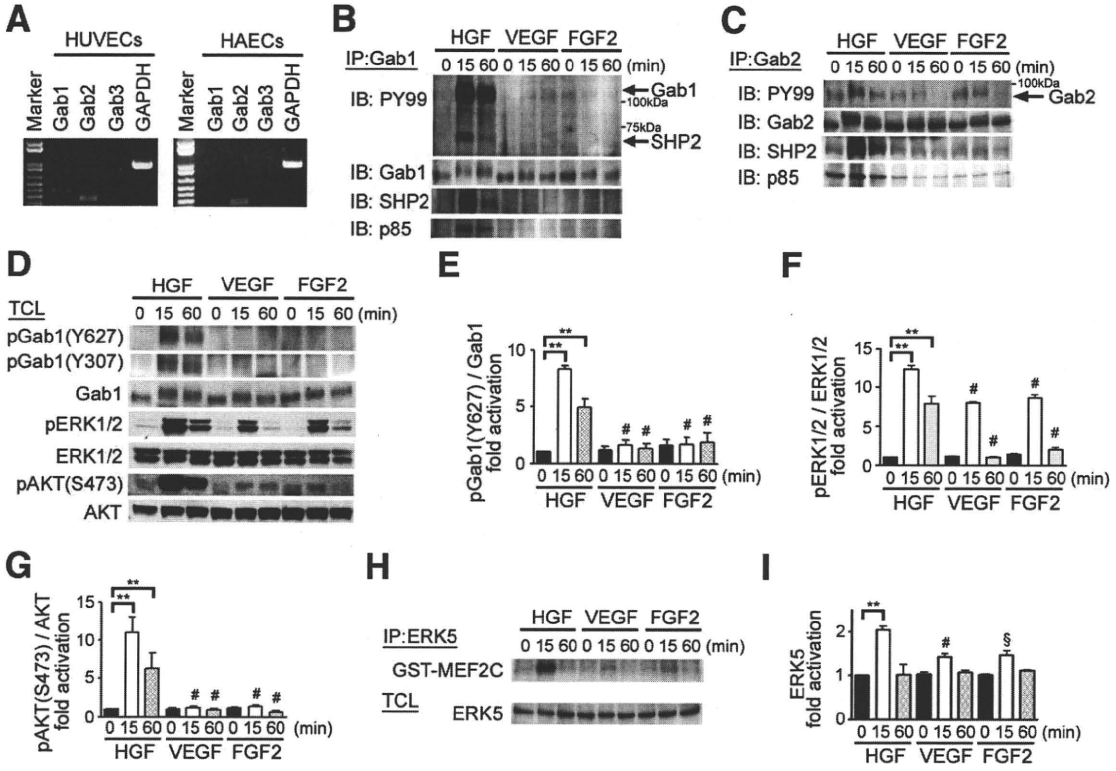


**Figure 2. Gab1 and its downstream signaling pathways are strongly activated after stimulation with HGF in HUVECs. A,** RT-PCR shows the expression of Gab1 and Gab2 mRNAs, but not Gab3 mRNA, in both HUVECs and human aortic ECs (HAECs). **B and C,** Tyrosine phosphorylation of Gab1 **(B)** and Gab2 **(C)** and their association with SHP2 and p85 were analyzed by immunoprecipitation of the HUVECs lysates. HUVECs were stimulated with HGF, VEGF, or FGF2 and cell lysates were subjected to immunoprecipitation with anti-Gab1 **(B)** or anti-Gab2 **(C)** serum, followed by immunoblotting analysis using the antibodies indicated at the **left. D,** Phosphorylation of Gab1 on Tyr-627 or Tyr-307, ERK1/2, and AKT were assessed by phosphor-specific antibodies. **E,** Phosphorylation of Gab1 on Tyr-627 was quantified against total Gab1 (n=3). **F,** Phosphorylation of ERK1/2 was quantified against total ERK1/2 (n=3). **G,** Phosphorylation of AKT (Ser473) was quantified against total AKT (n=3). **H,** ERK5 activity was measured by in vitro kinase assay using anti-ERK5 immunoprecipitates from the corresponding cell lysates as described in Methods (n=3). $^{32}$P-labeled substrates are shown at the **top** (GST-MEF2C). In parallel, cell lysates were subjected to immunoblotting with anti-ERK5 antibody **(bottom)** to confirm the equal amount loading. **I,** ERK5 activity was quantified by scanning densitometry and was expressed relative to input ERK5 (total cell lysate). The results were expressed as relative intensity over cells treated with vehicle. $^{**}P<0.01$ for the indicated groups; $\#P<0.01$, $\S P<0.05$ vs HGF-treated cells at the same time after stimulation. Values are shown as means±SEM for 3 separate experiments.

ficity of this inhibition was demonstrated by the unaltered expression of ERK1/2 and AKT in each condition (Figure 3A). HGF-induced activation of ERK1/2, AKT, and ERK5 were significantly attenuated in HUVECs transfected with Gab1-specific siRNA compared with those transfected with control siRNA (Figure 3A through 3E). Conversely, HGF-induced activation of ERK1/2, AKT, and ERK5 were significantly enhanced in HUVECs transfected with Gab2-specific siRNA compared with those transfected with control siRNA (Figure 3A through 3E), suggesting that Gab2 might exert an inhibitory role for HGF/c-Met/Gab1-dependent signaling. These data indicate that Gab1 and Gab2 might have an opposite role for activation of ERK1/2, AKT, and ERK5 after HGF stimulation in HUVECs.

## Gab1 Has an Essential Role for HGF-Dependent Signaling Through Association With SHP2 and p85 in HUVECs

To delineate the role of Gab1 in HGF-dependent signaling, we used adenovirus vectors expressing β-galactosidase (β-gal) (control), wild-type Gab1 (Gab1$^{WT}$), mutated Gab1 that is unable to bind SHP2 (Gab1$^{\Delta SHP2}$), or mutated Gab1 that is unable to bind p85 (Gab1$^{\Delta p85}$), as described previously.[18,24] We found that Gab1 indeed associated with c-Met after stimulation with HGF in HUVECs overexpressing Gab1$^{WT}$ (Online Figure III). Next, we examined the effect of adenovirus-mediated forced expression of Gab1$^{WT}$, Gab1$^{\Delta SHP2}$, or Gab1$^{\Delta p85}$ on the HGF-dependent downstream signaling pathways. HGF induced activation of ERK1/2, AKT, and ERK5 in the control HUVECs expressing β-gal (Figure 4A and 4D). Whereas HGF-induced activation of ERK1/2 was augmented in HUVECs expressing Gab1$^{WT}$ or Gab1$^{\Delta p85}$ compared with control cells expressing β-gal, activation of ERK1/2 was significantly attenuated in HUVECs expressing Gab1$^{\Delta SHP2}$ (Figure 4A and 4B). Furthermore, HGF-induced activation of ERK5 was enhanced in HUVECs expressing Gab1$^{WT}$ compared with control cells expressing β-gal. In addition, enhanced activation of ERK5 was abrogated in HUVECs expressing Gab1$^{\Delta SHP2}$ compared with cells expressing Gab1$^{WT}$ (Figure 4D and 4E). Therefore, the complex formation of Gab1 with SHP2 is required not only for activation of ERK1/2 but also for that of ERK5 after stimulation with HGF in HUVECs.

On the other hand, HGF-induced activation of AKT was significantly enhanced in HUVECs expressing Gab1$^{WT}$ or

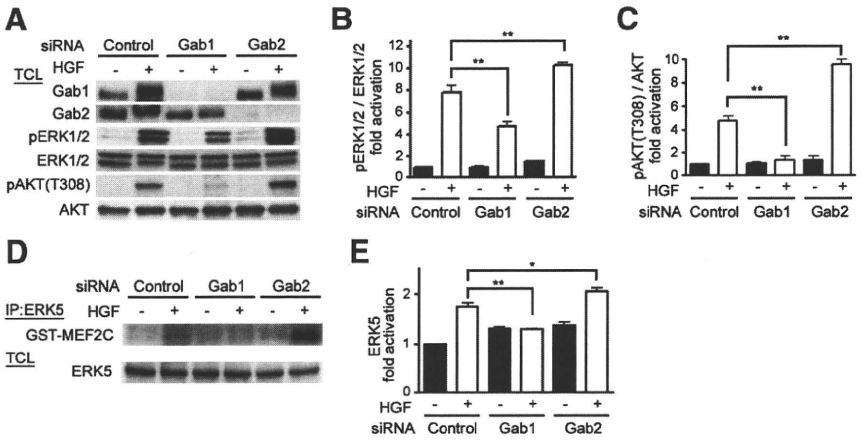


**Figure 3. siRNA-mediated knockdown of Gab1, but not Gab2, significantly attenuates activation of ERK1/2, AKT, and ERK5 in response to HGF in HUVECs. A,** HUVECs were transfected with control siRNA (Control) or siRNAs targeting either Gab1 or Gab2 for 48 hours. After serum starvation, HUVECs were treated with HGF (20 ng/mL) for 15 minutes. Activation levels of ERK1/2 and AKT were assessed by phospho-specific antibodies. Activation of ERK1/2 and AKT was attenuated in HUVECs transfected with the siRNA targeting Gab1, but enhanced with that targeting Gab2, compared with control cells. **B,** Phosphorylation of ERK1/2 was quantified against total ERK1/2 (n=3). **C,** Phosphorylation of AKT (Ser-473) was quantified against total AKT (n=3). **D,** ERK5 activity was measured by in vitro kinase assay using anti-ERK5 immunoprecipitates from the corresponding cell lysates almost similarly described in Figure 2H (n=3). $^{32}$P-labeled substrates are shown at the **top** (GST-MEF2C). In parallel, cell lysates were subjected to immunoblotting with anti-ERK5 antibody **(bottom)** to confirm the equal amount loading. **E,** ERK5 activity was quantified by scanning densitometry and was expressed relative to input ERK5 (total cell lysate). The results were expressed as relative intensity over cells treated with vehicle. $^{*}P<0.05$, $^{**}P<0.01$ for the indicated groups. Values are shown as means±SEM for 3 separate experiments.

Gab1$^{\Delta SHP2}$ compared with control cells, but not in cells expressing Gab1$^{\Delta p85}$ (Figure 4A and 4C). Hence, the complex formation of Gab1 with p85 is critically involved in activation of AKT after stimulation with HGF in HUVECs.

## HGF Induces EC Migration via Complex Formation of Gab1 With SHP2 and With p85

Next, we examined HGF-dependent EC migration as an in vitro model for the angiogenic response. HUVECs were infected with adenovirus vectors expressing β-gal, Gab1$^{WT}$, Gab1$^{\Delta SHP2}$, or Gab1$^{\Delta p85}$, and the effect of forced expression of various Gab1 proteins was examined in a monolayer "wound injury" assay. HGF-induced EC migration was significantly enhanced by overexpression of Gab1$^{WT}$, but significantly repressed by that of Gab1$^{\Delta SHP2}$, compared with control cells expressing β-gal (Figure 4F and 4G). In addition, overexpression of Gab1$^{\Delta p85}$ slightly reduced HGF-induced EC migration, compared with control cells (Figure 4F and 4G). These findings indicate that Gab1 regulates HGF-induced EC migration predominantly via complex formation with SHP2 and partly via that with p85.

To further delineate the downstream signaling pathways of Gab1-SHP2 complex responsible for HGF-induced EC migration, HUVECs were infected with adenovirus vectors expressing dominant-negative MAPK/ERK5 (MEK5$^{DN}$), dominant-negative ERK5 (ERK5$^{DN}$), or dominant-negative MAPK/ERK1 (MEK1$^{DN}$). HGF-induced endothelial migration was almost abrogated by overexpression of MEK1$^{DN}$, but not by that of MEK5$^{DN}$ or ERK5$^{DN}$ (Online Figure IV, A and B). In addition, we examined the effect of overexpression of constitutive-active MEK5 (MEK5$^{CA}$) or constitutive-active MEK1 (MEK1$^{CA}$) on the cell migration of HUVECs overexpressing Gab1$^{\Delta SHP2}$. Overexpression of MEK1$^{CA}$, but not MEK5$^{CA}$, restored cell migration of the HUVECs overexpressing of Gab1$^{\Delta SHP2}$ (Online Figure IV, C and D). Taken together, these findings indicate that MEK1/2-ERK1/2, but not MEK5-ERK5, is responsible for HGF-induced EC migration via Gab1-SHP2 complex.

## HGF Stimulation Leads to a Distinct Pattern of Gene Expression via Gab1 in HUVECs

To explore the potential downstream target genes of HGF/c-Met/Gab1 signaling in the vascular endothelium, we used DNA microarrays to carry out a global survey of mRNA in HUVECs overexpressing various Gab1 proteins treated with or without HGF for 1 hour. Several transcripts were upregulated in response to HGF stimulation in the cells overexpressing Gab1$^{WT}$, but not in those overexpressing either Gab1$^{\Delta SHP2}$ or Gab1$^{\Delta p85}$ (Figure 5A). Because both Gab1-SHP2 and Gab1-p85 complex formation are prerequisite for HGF-induced EC migration as demonstrated in Figure 4F and 4G, we focused on these genes, which were upregulated by overexpression of Gab1$^{WT}$, but not that of Gab1$^{\Delta SHP2}$ or Gab1$^{\Delta p85}$, as presented in the cluster diagram (Figure 5A). By quantitative real-time RT-PCR, we confirmed that *KLF2*, *Egr1* (early growth response 1), *Egr3*, and *COX2* (cyclooxygenase-2) were indeed upregulated in HUVECs overexpressing Gab1$^{WT}$, but not in those overexpressing Gab1$^{\Delta SHP2}$ (Figure 5B through 5E). Almost similar results were validated by immunoblotting analysis especially for the expression of KLF2 and Egr1 (Figure 5F).

KLF2 has important roles for vascular endothelial homeostasis downstream of several proangiogenic factors, laminar fluid shear stress, and statins.[16] In addition, Egr1 has also been reported to be critical for ischemia-related gene regulation in the vascular endothelium.[25,26] Thus, we performed further analysis focusing on these 2 genes. To confirm the involvement of Gab1 in the gene regulation of *KLF2* and *Egr1*, we performed siRNA-mediated knockdown of Gab1 in HUVECs. HGF-induced upregulation of both *KLF2* and *Egr1* was abrogated by knockdown of Gab1, but not by that of Gab2 (Figure 5G and 5H). Almost similar result was obtained from immunoblotting analysis for the expression of KLF2 and Egr1 (Figure 5I). KLF2 has been reported to exert antithrombotic and antiinflammatory functions in part through upregulation of the thrombomodulin gene (*TM*).[16,27] Consistently, we confirmed that

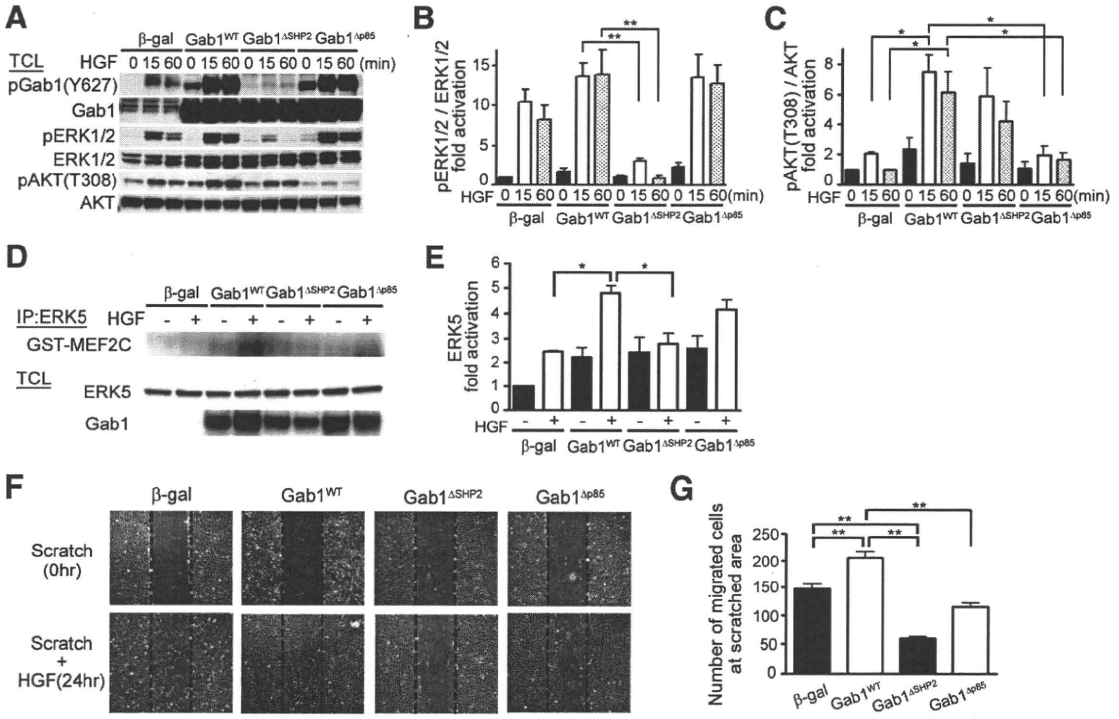


**Figure 4. Gab1 is essential for activation of ERK1/2, AKT, and ERK5 and subsequent cell migration after HGF stimulation in HUVECs. A,** HUVECs, infected with the indicated adenovirus vectors, were stimulated with HGF (20 ng/mL). Cell lysates were collected and subjected to immunoblotting analyses using the antibodies indicated at the **left**. Expression level of Gab1 was almost comparable in the cells overexpressing Gab1$^{WT}$, Gab1$^{\Delta SHP2}$, or Gab1$^{\Delta p85}$. Phosphorylation of Gab1 on Tyr-627 was almost abrogated in the cells overexpressing Gab1$^{\Delta SHP2}$. **B,** Phosphorylation of ERK1/2 was quantified against total ERK1/2 (n=3). **C,** Phosphorylation of AKT (Thr308) was quantified against total AKT (n=3). **D,** ERK5 activity was measured by in vitro kinase assay almost similarly described in Figure 2H (n=3). $^{32}$P-labeled substrates are shown at the **top** (GST-MEF2C). In parallel, cell lysates were subjected to immunoblotting with anti-ERK5 antibody to confirm the equal amount loading **(middle)** and with anti-Gab1 antibody to verify the overexpression of Gab1 **(bottom). E,** ERK5 activity was quantified and expressed relative to input ERK5 (total cell lysate). The results were expressed as relative intensity over cells expressing β-gal treated with vehicle. **F,** HUVECs infected with the indicated adenovirus vectors were serum-starved and subjected to "wound injury" assay by scratching. Cells were treated with or without HGF (50 ng/mL) for 24 hours. **G,** Quantification for EC migration in "wound injury" assay. *$P$<0.05, **$P$<0.01 for the indicated groups. Values are shown as means±SEM for 3 separate experiments.

*TM* was indeed upregulated in HUVECs overexpressing Gab1$^{WT}$, but not in those overexpressing Gab1$^{\Delta SHP2}$ at 4 hours after stimulation with HGF in HUVECs (Online Figure V, A), suggesting that Gab1 might be involved in antithrombotic function through KLF2/TM pathway downstream of HGF/c-Met in the ECs.

To reveal the signaling pathways responsible for gene expression of *KLF2* and *Egr1*, HUVECs were infected with adenovirus vectors expressing MEK5$^{DN}$, ERK5$^{DN}$, or MEK1$^{DN}$. HGF-induced upregulation of *KLF2* was almost abrogated by overexpression of either MEK5$^{DN}$ or ERK5$^{DN}$, but not by that of MEK1$^{DN}$, suggesting that HGF upregulates *KLF2* gene via MEK5-ERK5 pathway (Online Figure V, B). Conversely, HGF-induced upregulation of *Egr1* was suppressed by overexpression of MEK1$^{DN}$, but not by overexpression of either MEK5$^{DN}$ or ERK5$^{DN}$, suggesting that HGF induces upregulation of *Egr1* through MEK1/2-ERK1/2 pathway (Online Figure V, C). These findings suggest that Gab1-SHP2 complex regulates HGF-induced upregulation of *KLF2* and *Egr1*, via ERK5 and via ERK1/2, respectively.

## Gab1 Is Essential for HGF-Induced In Vivo Postnatal Angiogenesis

We confirmed whether ischemia-induced angiogenesis was associated with a rise in HGF expression in the ischemic tissues. Ischemic tissues were harvested at the indicated time and subjected to ELISA. In control mice (Gab1$^{flox/flox}$), a rise in HGF expression was observed in the ischemic tissues from 12 to 48 hours after HLI (Figure 6A). HGF expression levels in the ischemic limbs of control and Gab1ECKO mice were almost comparable at 24 hours after HLI by immunoblotting analysis (Online Figure VI, A and B). Almost similarly, VEGF expression levels in those of both control and Gab1ECKO mice were also almost similar at 24 hours after HLI (Online Figure VI, A and C).

We next evaluated the effect of HGF and VEGF gene transfer in HLI model in both control and Gab1ECKO mice. The vacant plasmid (pVAX1; control) and the expression plasmids of human HGF (pVAX1-HGF) and human VEGF$_{165}$ (pVAX1-VEGF) were introduced after HLI as described in Methods. In control mice, injection of both pVAX1-HGF and pVAX1-VEGF plasmids into ischemic limbs significantly enhanced blood flow recovery on day 21 after HLI, compared with the pVAX1-injected group (Figure 6B and 6C). Intriguingly, in Gab1ECKO mice, injection of pVAX1-VEGF into ischemic limbs significantly augmented blood flow recovery on day14 and 21 after HLI, whereas injection of pVAX1-HGF did not increase blood flow recovery (Figure 6B and 6C). Consistent with these findings obtained from LDBF

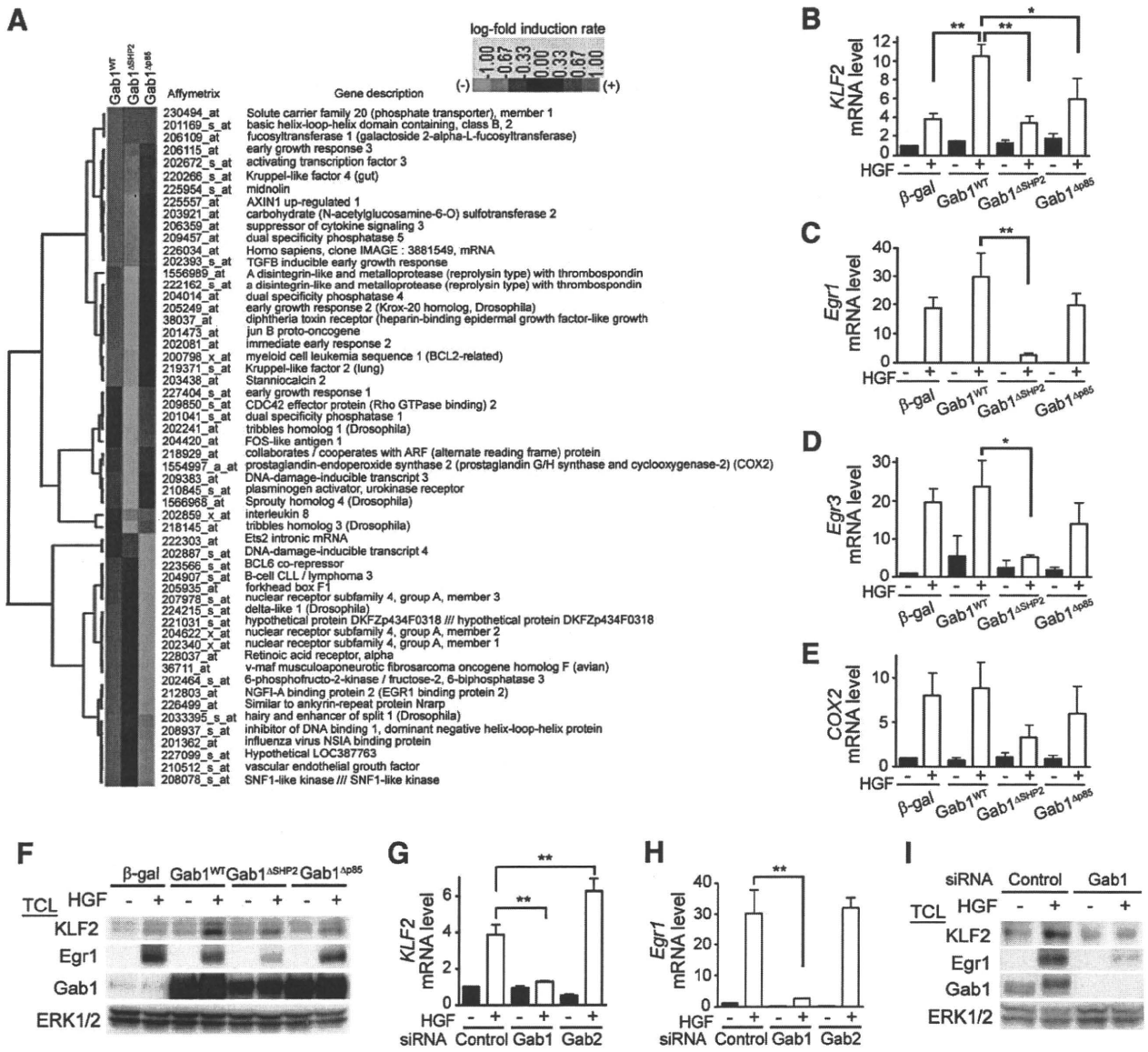


**Figure 5. HGF stimulation leads to a distinct pattern of gene expression via Gab1. A,** HUVECs infected with the indicated adenovirus vectors were serum-starved and treated with vehicle or 20 ng/mL HGF for 1 hour. Total RNA was purified from the HUVECs and subjected to Affymetrix microarray analysis. Genes corresponding to the criteria described in Methods were subjected to the cluster analysis. **Red and green** represent higher and lower expression than the median for that particular gene, respectively. Color intensity is related to the difference with the median **(black). B through E,** Total RNA was purified from the HUVECs treated with vehicle (−) or 20 ng/mL HGF (+) for 1 hour. The expression levels of *KLF2* **(B),** *Egr1* **(C),** *Egr3* **(D),** and *COX2* **(E)** were analyzed by real-time RT-PCR. **Bar graphs** show relative RNA levels of each gene normalized to GAPDH levels. RNA levels are expressed relative to that in cells expressing β-gal treated with vehicle. **F,** Cell lysates treated with vehicle (−) or HGF (+) for 1 hour were subjected to immunoblotting analyses. **G and H,** HUVECs, transfected with control siRNA (control) or siRNAs targeting either Gab1 or Gab2, were treated with vehicle (−) or HGF (+) for 1 hour. Expression levels of *KLF2* **(G)** and *Egr1* **(H)** mRNAs were analyzed as described for **B through E. I,** Cell lysates treated with vehicle (−) or HGF (+) for 1 hour were subjected to immunoblotting analyses. Values are shown as means±SEM for 3 separate experiments. $^{**}P<0.01$, $^{*}P<0.05$ for the indicated groups.

analysis, injection of pVAX1-VEGF rescued 60% of limb necrosis in Gab1ECKO mice, whereas injection of pVAX1-HGF could only rescue 25% of limb necrosis in Gab1ECKO mice (Figure 6D). These data indicate that Gab1 is more strongly involved in HGF-dependent angiogenesis than in VEGF-dependent angiogenesis in vivo.

To validate the expression of downstream target genes of Gab1 in the endothelium, we purified CD31-positive ECs from both control and Gab1ECKO mice both at baseline and on day 1 after HLI. The expression of KLF2 and Egr1 in the vascular endothelium significantly decreased in Gab1ECKO mice compared with control mice, whereas the expression of CD31 and cyclophilin A was almost comparable between control and Gab1ECKO mice (Figure 6E through 6G). In addition, the expression of *TM* mRNA in the vascular endothelium significantly decreased in Gab1ECKO mice compared with control mice (Online Figure VII, A and B). Taken together, these findings suggest that HGF/c-Met/Gab1-dependent signaling was virtually attenuated both at baseline and after ischemia in